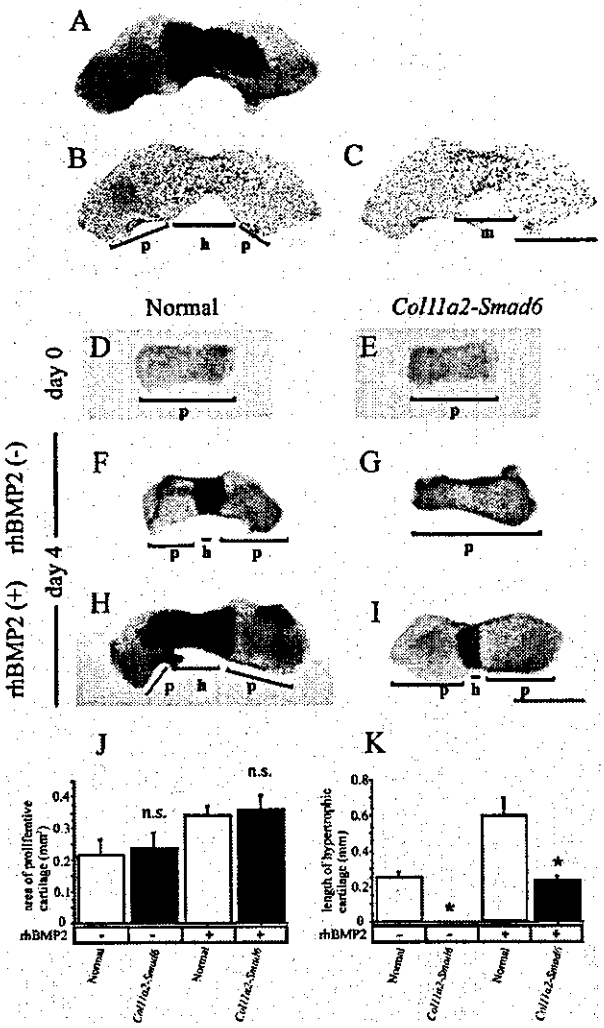

Figure 8. **Down-regulation of chondrocyte hypertrophy induced by rhBMP2 in cartilage explants by Smad6 overexpression.** (A–C) Microscopic and histological appearance of normal mouse metatarsal rudiments cultured in the presence of rhBMP2. (A) Rudiments consist of bright gray areas at both ends and dark gray central areas under phase-contrast microscopy. (B) Histological section stained with safranin O shows that bright and dark gray areas correspond to proliferative and hypertrophic cartilage, respectively. (C) von Kossa staining shows that dark gray areas contain mineralized tissue. (D–I) Cultured metatarsal rudiments prepared from normal (D, F, and H) and Smad6 transgenic (E, G, and I) mice. (D and E) Rudiments at the start of culture. (F and G) Rudiments cultured for 4 d in control medium. (H and I) Rudiments cultured for 1 d in control medium followed by 3 d in medium containing rhBMP2. (J and K) Morphometric analysis of metatarsal explant. Areas of proliferative cartilage and length of hypertrophic cartilage were measured for each rudiment. Error bars show means ± SD (n = 5). p, Proliferative cartilage; h, hypertrophic cartilage; m, mineralized hypertrophic cartilage; n.s., not significant. *, $P < 0.01$ between normal and transgenic mice as determined by one-way analysis of variance (ANOVA) followed by Fisher's PLSD test. Bars (A–I), 500 μm.

the femur was significantly shorter in Smad6 transgenic mice than in normal mice. Furthermore, the mineralized area in the femur was significantly shorter in Smad6/Smurf1 double-transgenic mice than in Smad6 transgenic mice. (Fig. 9, C–G). Histological analysis revealed that ossification was further delayed in the double-transgenic mice compared with the Smad6 transgenic mice (Fig. 9, H and I). Labeling cartilage with BrdU revealed little differences in chondrocyte proliferation among normal littermates and the single- or double-transgenic mice. The labeling indexes at 16.5 d.p.c. were 7.66 ± 1.51, 7.86 ± 1.05, 7.65 ± 1.12, and 7.31 ± 3.74 cells/0.01 mm^2 cartilage in normal littermates, Smurf1 transgenic, Smad6 transgenic, and Smad6/Smurf1 double-transgenic mice, respectively (no significant difference; n = 5, $P > 0.05$).

Discussion

Smad6 controls chondrocyte hypertrophy by down-regulating BMP signals in endochondral ossification

Mice lacking Smad6 develop cardiovascular abnormalities (Galvin et al., 2000). Ectopic endochondral bone forms in the heart of mutant mice, suggesting that Smad6 plays certain roles in endochondral bone formation in vivo. However, the physiological roles of Smad6 and Smad signaling in normal endochondral bone formation are poorly understood. In this work, we generated transgenic mice overexpressing Smad6 in chondrocytes. Smad6 overexpression resulted in a delayed chondrocyte hypertrophy and mineralization in endochondral ossification. Smad1/5/8 phosphorylation was inhibited in Smad6 transgenic cartilage, suggesting that Smad signaling was impaired in these mice.

Smad6 appears to block BMP signaling, whereas Smad7 blocks that of both TGF-β and BMP (Hanyu et al., 2001). Skeletal mineralization is delayed and skeletal patterning is defective in mice lacking growth and differentiation factor 5 (Storm et al., 1994), BMPR-IB (Yi et al., 2000), or BMP7 (Luo et al., 1995; Jena et al., 1997). The similarity of delayed mineralization between these mutant mice and Smad6 transgenic mice suggests that BMP signals are blocked by Smad6 during endochondral ossification. This notion was confirmed by our results that chondrocyte hypertrophy and mineralization induced by rhBMP2 was inhibited in cartilage explants from Smad6 transgenic mice. Because the phosphorylation of Smad1/5/8 induced by rhBMP2 was inhibited in explants from Smad6 transgenic mice, we concluded that Smad6 regulates chondrocyte hypertrophy through the inhibition of Smad1/5/8 phosphorylation, thus down-regulating BMP signaling in endochondral bone formation.

The most fundamental abnormality during chondrocyte differentiation in Smad6 transgenic mice was a delay in chondrocyte hypertrophy in humeri at 14.5 d.p.c. This delay was accompanied by the persistent expression of the *Col2a1* gene and the retarded expression of the type X collagen gene (*Col10a1*). Extensive analyses in vitro have shown that BMP signals promote chondrocyte hypertrophy, and BMP-responsive cis-acting elements have been identified in the promoter sequence of the *Col10a1* gene (Volk et al., 1998; Drissi et al., 2003). These in vitro analyses and our in vivo results collectively suggest that Smad6 overexpression blocks BMP signaling, thus preventing transcriptional activation of the *Col10a1* gene.

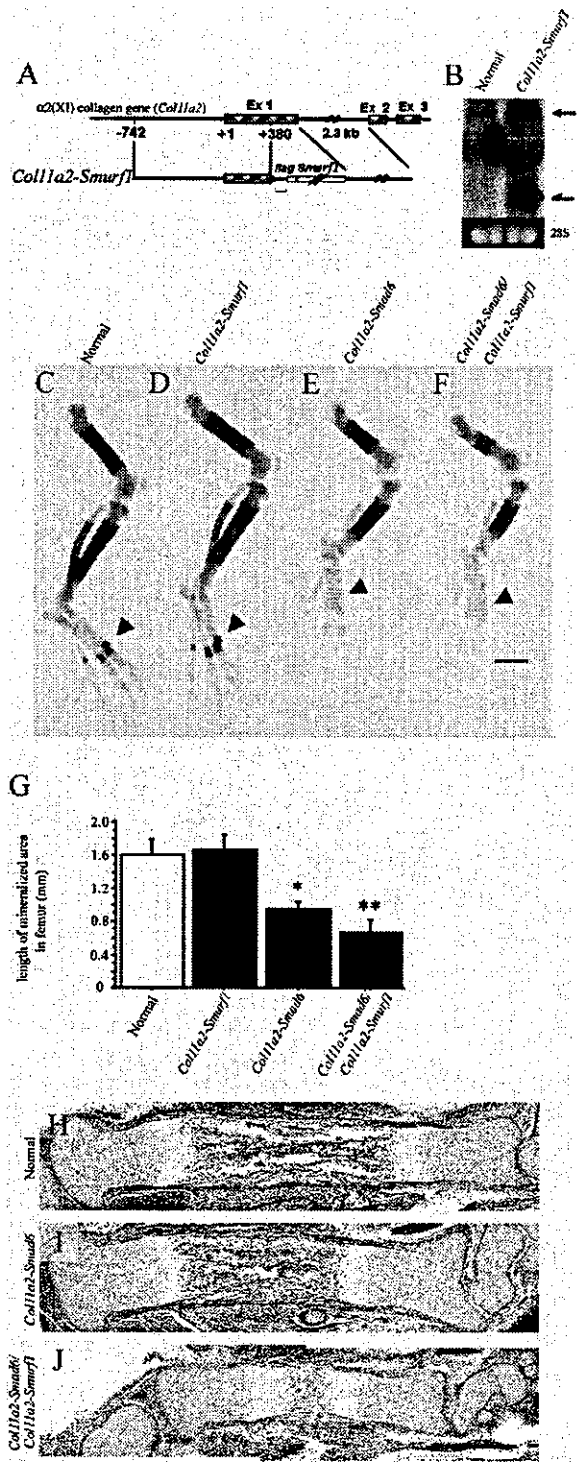

Figure 9. **Skeletal phenotypes are more severely disrupted in Smad6/Smurf1 double-transgenic mice than in Smad6 transgenic mice.** (A) DNA constructs used to generate Smurf1 transgenic mice. Gene structure of *Col11a2* is shown at top. (B) Northern blot hybridized with Smurf1 probe. Left, wild-type; right, Smurf1 transgenic mice. Bottom shows ethidium bromide–stained gel before transfer. (C–F) Alcian blue and Alizarin red S staining of hindlimb skeleton of normal (C), Smurf1 transgenic (D), Smad6 transgenic (E), and Smad6/Smurf1 double-transgenic (F) mice at 16.5 d.p.c. (G) Length of mineralized area in femur at 16.5 d.p.c. Length of tissue stained with Alizarin red S was measured. (H–J) Histology of tibia of normal (H), Smad6 transgenic (I), and Smad6/Smurf1 double-transgenic (J) mice at 16.5 d.p.c. Arrow shows endogenous Smurf1 mRNA. Half-arrow indicates Smurf1 transgene mRNA. Arrowheads indicate mineralized tissues in metatarsals. Error bars show means ± SD ($n = 5$). *, $P < 0.01$ between normal and Smad6 transgenic mice; **, $P < 0.01$ between Smad6 transgenic and Smad6/Smurf1 double-transgenic mice as determined by one-way analysis of variance (ANOVA) followed by Fisher's PLSD test. Bars (C–F and H–J), 0.5 mm.

Smad6 regulates endochondral ossification in cooperation with Smurf1

Smurf1 binds Smads 1 and 5 and promotes their degradation (Zhu et al., 1999). Smurf1 and Smad6 form complexes and inhibit BMP signaling through the ubiquitin-dependent degradation of BMP receptors as well as of R-Smads (Murakami et al., 2003). Smurf2 may also exhibit functions similar to Smurf1. To examine the in vivo function of Smurf1, we generated transgenic mice expressing Smurf1 in chondrocytes and did not find obvious abnormalities. These results suggest that sufficient Smurf1 already exists in normal chondrocytes. When apparently normal Smurf1 transgenic mice were mated with Smad6 transgenic mice, the endochondral ossification of progenies overexpressing both Smad6 and Smurf1 was more delayed than in transgenic mice overexpressing only Smad6. It is likely that the Smad6 transgenic mice have far less Smurf1/2 than Smad6. In Smad6/Smurf1 double-transgenic mice, Smurf1 derived from the transgene might compensate for this shortage, thus supporting the activities of a large amount of Smad6. When Smurf1 transgenic mice were mated with those of the Smad6 transgenic line 165 in which the expression level was low, the phenotypic severity of the resultant double-transgenic progeny did not differ from those of Smad6 transgenic mice of line 165 (unpublished data). In Smad6 transgenic mice of this line, endogenous Smurf1/2 fully supported the activities of endogenous Smad6 and that derived from the transgene. From these lines of discussion, the expression level of Smad6 appears to be critical in the regulation of conversion from proliferative chondrocytes to hypertrophic chondrocytes. Actually, the expression level of Smad6 is decreased in the transitional zone between proliferative chondrocytes and hypertrophic chondrocytes (Flanders et al., 2001), suggesting that critical regulation of Smad6 expression is responsible for this conversion. The expression level of inhibitory Smads seems to be consistently and strictly regulated through autoregulatory negative feedback during signal transduction of the TGF-β/BMP superfamily because the inhibitory Smad mRNA is induced by TGF-β stimulation (Heldin et al., 1997).

Postnatal dwarfism with osteopenia might be associated with the reduced zone of hypertrophic chondrocytes

The most apparent phenotype of Smad6 transgenic mice was postnatal dwarfism and osteopenia. Dynamic bone histomorphometric analysis revealed that osteoblastic bone formation decreased and that osteoclastic bone resorption increased in Smad6 transgenic mice. However, results from cultured bone marrow cells suggested normal osteoclast-sup-

porting activities of osteoblasts/stromal cells prepared from Smad6 transgenic mice. These in vitro results suggest that the increased in vivo osteoclastic bone resorption in transgenic mice was not due to an autonomous abnormality within bone marrow cells. This notion was consistent with the observation that the transgene was specifically expressed in chondrocytes. We speculate that abnormal activities of osteoblasts and osteoclasts might be associated with the dysfunction in cartilage during endochondral bone formation. However, we could not rigorously exclude leaky transgene expression in cells in osteoblast lineage, and thus the possibility that osteoblasts have a primary malfunction.

BrdU labeling revealed that proliferation of chondrocytes in Smad6 transgenic mice was normal at the embryonic stage and at the postnatal stage. Therefore, postnatal dwarfism in Smad6 transgenic mice might develop through a different mechanism from that in transgenic mice overexpressing activated FGF receptor 3 in cartilage, in which chondrocyte proliferation is normal in embryos but postnatally decreased (Naski et al., 1998).

The onset of chondrocyte hypertrophy was delayed by ~3 d during the development of Smad6 transgenic mice. Once the zone of hypertrophic chondrocytes formed, the height of the zone of hypertrophic chondrocytes was essentially normal, suggesting that the population of hypertrophic chondrocytes is strictly regulated at late embryonic stages. We did not determine which mechanism maintains the population of hypertrophic chondrocytes in Smad6 transgenic embryos. However, this population decreased in the transgenic mice after birth. It is likely that reduced hypertrophic chondrocyte population lead to a deficiency in signals required for coordination of growth and bone formation after birth. Hypertrophic chondrocytes are known to produce various factors, including angiogenic factors (Karsenty and Wagner, 2002). A reduction in production of such factors may well lead to dysfunction of osteoblast/osteoclast activities, thus resulting in impaired bone growth and osteopenia.

It is also possible that abnormal chondrocyte hypertrophy could result in the impaired structure of the ECM of hypertrophic cartilage. An impaired matrix might not provide a suitable scaffold for osteoblasts and osteoclasts to replace cartilage with bone. This speculation remains to be examined.

Chondrocyte proliferation was not affected in Smad6 transgenic mice

Previously, we generated transgenic mice expressing noggin in chondrocytes under the control of the identical *Col11a2* promoter/enhancer sequences used in this paper (Tsumaki et al., 2002). We examined 62 G_0 founder mouse embryos for the noggin transgene, and 7 of them displayed a severe phenotype and almost completely lacked cartilage formation during development. On the other hand, 17 of 129 G_0 embryos were genetically positive for the Smad6 transgene, and skeletal abnormalities were either relatively minor or almost absent. Although we could not exclude the possibility that the phenotypic difference between noggin and Smad6 transgenic mice might be related to the different level of expression of the transgenes, these results suggest that noggin tends to affect cartilage more than Smad6 when expressed in chondrocytes in transgenic mice.

In addition, chondrocyte proliferation is inhibited in mice lacking BMPR-IB (Yi et al., 2000) and in cartilage explants cultured in the presence of noggin (Minina et al., 2001). Reports have consistently indicated that BMP signaling stimulates chondrocyte proliferation during endochondral bone formation at the embryonic stages of transgenic mice overexpressing BMPs in cartilage (Tsumaki et al., 1999, 2002) and in organ culture of cartilage rudiments in the presence of BMPs (De Luca et al., 2001; Minina et al., 2001).

On the other hand, chondrocyte proliferation appeared normal in Smad6 transgenic mice, as indicated by BrdU labeling. For explanation of the discrepancy between the findings of chondrocyte proliferation obtained from Smad6 transgenic mice and those of other papers, we considered four possibilities. First, we could not exclude the possibility that the expression level of Smad6 transgene was not sufficient to block BMP signaling completely, although immunohistochemical analysis showed strong expression of the transgene (Fig. 2, C–J) Second, Smad signaling might not be blocked by Smad6 alone. Certainly, phenotypes of Smad6/Smurf1 double-transgenic mice were more severe than that of Smad6 transgenic mice. However, it is still milder than that of noggin transgenic mice, and chondrocyte proliferation remained normal, as indicated by BrdU labeling. Third, BMP signals might be mediated by signaling pathways other than Smad proteins. In certain cell types, various MAPKs have been reported to mediate BMP pathways (Iwasaki et al., 1999). Existence of such pathways might account for the discrepancy between chondrocyte proliferation in BMPR-IB–deficient mice and Smad6 transgenic mice. There is likelihood of the fourth possibility as follows: BMPs and noggin are secreted and diffuse. In addition to direct binding to chondrocytes, these proteins might exert indirect effects on chondrocytes. For example, BMPs act on cells around cartilage, and in return these cells secrete factors, affecting chondrocyte proliferation. Thus, the addition or overexpression of BMPs/noggin modulate chondrocyte proliferation directly and indirectly. On the other hand, Smad6 overexpression in chondrocytes might block only the direct effect of BMPs on chondrocytes.

In conclusion, our data on inhibition of endochondral bone formation in Smad6 and Smurf1 transgenic mice suggest a role for Smad signaling in skeletogenesis and growth. By down-regulating Smad1/5/8 phosphorylation and BMP signals, Smad6 plays an important role in regulation of chondrocyte hypertrophy and synergistically cooperates with Smurf1 in vivo.

Materials and methods

Construction of the transgene

The α2(XI) collagen gene–based expression vector, 742*lacZ*Int, contains the *Col11a2* promoter (−742 to +380), an SV40 RNA splice site, the β-galactosidase reporter gene, the SV40 polyadenylation signal, and 2.3 kb of the first intron sequence of *Col11a2* as an enhancer (Tsumaki et al., 1996). To create a Smad6 transgene, a 1.5-kb DNA fragment covering the entire coding region of mouse Smad6 cDNA tagged with a FLAG sequence at the NH_2 terminus was prepared. The FLAG-tagged Smad6 cDNA was cloned into the NotI sites of 742*lacZ*Int expression vectors by replacing the β-galactosidase gene to create *Col11a2-Smad6*. For the Smurf1 transgene, a FLAG-tagged Smurf1 cDNA was cloned into NotI sites of the expression vectors 742*lacZ*Int by replacing the β-galactosidase gene to create *Col11a2-Smurf1*.

Generation of transgenic mice

The plasmids *Col11a2-Smad6* and *Col11a2-Smurf1* were digested with EcoRI and PstI to release the inserts. Transgenic mice were produced by microinjecting each of the inserts into the pronuclei of fertilized eggs from F1 hybrid mice (C57BL/6x DBA) as described previously (Tsumaki et al., 1996). Transgenic embryos were identified by PCR assays of genomic DNA extracted from the placenta or skin. Genomic DNA was amplified by transgene-specific PCR using primers derived from mouse Smad6 cDNA (5′-CAAGATCGGTTTTGGCATACTG-3′) and from the SV40 poly(A) signal region (5′-TCACTGCATTCTAGTTGTGGTTTGTCC-3′) to amplify a 411-bp product for Smad6 transgenic mice. To discriminate Smurf1 transgenic mice, genomic DNA was amplified by transgene-specific PCR using primers derived from mouse Smurf1 cDNA (5′-ATGGACTACAAGGACGATGATGACAAGG-3′ and 5′-AGGGGCTGGTTCCTCCATGAAGCAG-3′) to amplify a 570-bp product. Smad6/Smurf1 double-transgenic pups were generated by mating Smad6 and Smurf1 transgenic mice.

Staining of the skeleton

Mice were dissected and fixed in 100% ethanol overnight, and then stained with Alcian blue followed by Alizarin red S solution according to standard protocols (Peters, 1977).

Micro CT analysis and bone mass measurement

The humeri from 5-wk-old transgenic mice and normal littermates were dissected and analyzed using a micro-focus X-ray CT system (SMX-100CT-SV; Shimadzu). The region extending from the proximal growth plate to the metaphyseal part of the humerus on 350 slices was scanned at a width of 6.75 μm per slice. The data were reconstructed to produce images of the humerus using 3-D visualization and measurement software (Vay Tek, Inc.). Bone mass was quantified by selecting 90 consecutive slices distal to the proximal growth plate (0.6 mm in length). Trabecular parameters in the metaphysis were determined using image analysis software (TRI/3D-BON; RATOC).

Histology and immunohistochemical staining

Embryos were dissected using a stereomicroscope (model SMZ645; Nikon), fixed in 4% PFA, processed, and embedded in paraffin. Serial sections were stained with hematoxylin and eosin, with safranin O/fast green/iron hematoxylin, or by the von Kossa reaction. Dynamic histomorphometric indices were determined by double-fluorescence labeling in vertebral bodies. 4-wk-old normal and transgenic mice were administered i.p. with tetracycline (20 mg/kg body weight; Sigma-Aldrich), followed by calcein label (10 mg/kg body weight; Wako Chemicals) 2 d later. After 24 h, the mice were killed. Bones were fixed with ethanol and embedded in methylmethacrylate. Sections were cut and viewed using a fluorescence microscope (Eclipse E1000; Nikon). The Niigata Bone Science Institute (Niigata, Japan) performed histomorphometric analyses. Immunohistochemistry proceeded using a rabbit pAb against Smad6 (1:200 dilution; Zymed Laboratories) and a rabbit pAb against phospho-Smad1/5/8 (1:200 dilution; Cell Signaling Technology). Immune complexes were detected using streptavidin-peroxidase staining and Histofine SAB-PO kits (Nichirei). Images were acquired using a microscope (Eclipse E1000; Nikon) with a digital camera system (DXM1200; Nikon).

BrdU staining

Pregnant mice bearing 16.5 d.p.c. embryos and 3-wk-old mice were i.p. injected with BrdU labeling reagent (10 μl/g body weight; Zymed Laboratories). 2 h later, the mice were killed. Embryonic limb buds and tibia of the 3-wk-old mice were dissected and sectioned. Incorporated BrdU was detected using a BrdU staining kit (Zymed Laboratories) to distinguish actively proliferating cells. Tissue sections were measured using a micrometer, and the average number of BrdU-positive cells/mm^2 cartilage ± SD was calculated.

Northern hybridization and real-time quantitative RT-PCR

Total RNA extracted from the limb buds of 14.5–18.5 d.p.c. transgenic and normal embryos using RNeasy Mini Kits (QIAGEN) was fractionated by electrophoresis through formaldehyde agarose gels and transferred onto Nytran® membranes (Schleicher & Schuell Bioscience). Complementary DNAs (cDNAs) were labeled with [^{32}P]dCTP using Prime-it® II kits (Stratagene). The membranes were hybridized with ^{32}P-labeled Smad6 cDNA and rehybridized with ^{32}P-labeled probes for mouse α1(II) collagen, α1(IX) collagen, and *Sox9*.

Total RNAs were digested with DNase to eliminate any contaminating genomic DNA before real-time quantitative RT-PCR. 2 μg of total RNA was reverse transcribed into first-strand cDNA using OmniScript® reverse transcriptase (QIAGEN) and an oligo(dT)12-18 primer. The PCR amplification proceeded in 20 μl containing 1 μl of cDNA, 2 μl of SYBER Green™ Master Mix (QIAGEN), and 10 pmol of primers specific for Smad6 (5′-GATCCCCAAGCCAGACAGT-3′ and 5′-AGCCTCTTGAGCAGCGCGAGTA-3′) to generate a 126-bp product (GenBank/EMBL/DDBJ accession no. NM008542). The cDNA was amplified by 35 cycles using a LightCycler® quick system (Roche) according to the following protocol: 94°C for 15 s, 60°C for 20 s, and 72°C for 6 s, each with a temperature transition rate of 20°C, according to the manufacturer's instructions.

In situ hybridization

Digoxigenin-11 UTP-labeled single-strand RNA probes were prepared using a DIG RNA labeling kit (Boehringer) according to the manufacturer's instructions. We generated antisense and sense probes using α1(II) collagen, α1(X) collagen, and osteopontin cDNAs. Hybridization proceeded as described previously (Hirota et al., 1992; Conlon and Herrmann, 1993). A Genius detection system (Boehringer) detected signals according to the manufacturer's instructions.

Immunoprecipitation and Western blotting

Limb buds of 14.5 d.p.c transgenic and normal embryos were lysed with RIPA buffer (50 mM Tris, pH 7.4, 150 mM NaCl, 1% Nonidet P-40, 0.5% sodium deoxycholate, 0.1% SDS, and 10 mM DTT) supplemented with protease and phosphatase inhibitor cocktails (Sigma-Aldrich). The positive control consisted of COS7 cells transfected with the expression construct FLAG-Smad6 that was also lysed with RIPA buffer. The cell lysates were incubated with anti-Smad6 antibody (Zymed Laboratories) for 3 h at 4°C followed by an incubation with protein G–agarose beads (Roche) for 3 h at 4°C. After five washes with lysis buffer (20 mM Hepes, 150 mM NaCl, 10% glycerol, 1.5 mM $MgCl_2$, 1 mM EGTA, and 100 μM orthovanadate), 1× SDS sample buffer was added to the agarose beads. The samples were incubated for 5 min at 95°C, fractionated by 10% SDS-PAGE, transferred onto nitrocellulose membranes (Bio-Rad Laboratories), and Western blotted against anti-FLAG M2 mAb (Sigma-Aldrich). Immunocomplex bands were visualized using the ECL Western blotting detection system (Amersham Biosciences).

Bone marrow cell culture

Osteoclast formation and bone resorbing activity were determined using the modified method described in Azuma et al. (2000). In brief, bone marrow cells prepared from the femurs and tibias of 10-wk-old transgenic mice or wild-type control mice were suspended in α-modified essential medium containing 10% FBS, and were cultured in 48-well plates (10^6 cells/0.5 ml per well) for 7 d in the presence of 0.1 μM dexamethasone (Sigma-Aldrich) and 0.01 μM recombinant human parathyroid hormone (Peptide Institute, Inc.). Cells were then fixed and stained for TRAP using a TRAP staining kit (Hokudo) according to the manufacturer's recommendation. The number of multinucleated TRAP-positive cells with more than three nuclei was counted under a microscope (Eclipse TE300; Nikon). To examine calcified matrix resorption activity, 5×10^5 cells were cultured in 16-well hydroxyapatite-coated slides (Osteologic; Becton Dickinson) for 14 d, and the resorption area was calculated by computer-assisted image analysis.

Metatarsal explant culture

Metatarsal rudiments were cultured as described previously (Haaijman et al., 1997). Metatarsal rudiments were dissected from transgenic and normal embryos at 15.0 d.p.c. and cultured in α-modified essential medium without nucleosides (Invitrogen), supplemented with 0.05 mg/ml ascorbic acid (Sigma-Aldrich), 0.3 mg/ml L-glutamine (Merck), 0.05 mg/ml gentamycin (Invitrogen), 0.25 mg/ml Fungizone® (Invitrogen), 1 mM β-glycerophosphate (Merck), and 0.2% FBS (GIBCO BRL) in a humidified atmosphere of 5% CO_2 in air at 37°C. 1 d after starting the cultures, the rudiments were incubated in 400 μl of the same medium containing 500 ng/ml of rhBMP2 (Yamanouchi Pharmaceutical Co., Ltd.) or without rhBMP2 for a further 3 d. For immunohistochemical analysis using anti-phosphorylated Smad1/5/8, rudiments were sectioned before and after a 2-h incubation with rhBMP2. Images of rudiments obtained under inverted phase-contrast microscopy were analyzed morphometrically (Eclipse TE300; Nikon). Areas of proliferative cartilage and length of hypertrophic cartilage were measured using NIH Image software (National Institutes of Health, Bethesda, MD).

We are grateful to Tomoatsu Kimura and Riko Nishimura for critical dis-

cussion. We are indebted to Yuko Shikauchi, Yuri Inada, and Kaori Sudo for their commitment to this investigation. We thank Akemi Ito for the histomorphometric analysis and Hideki Tsuboi for bone marrow cell culture.

This work was supported in part by Scientific Research grant 15390458 from the Ministry of Education, Science and Culture of Japan; Health and Labor Sciences Research Grants of Japan; and the Grant of Japan Orthopaedic and Traumatology Foundation, Inc. (0126).

Submitted: 4 November 2003
Accepted: 30 March 2004

References

Azuma, Y., K. Kaji, R. Katogi, S. Takeshita, and A. Kudo. 2000. Tumor necrosis factor-α induces differentiation of and bone resorption by osteoclasts. *J. Biol. Chem.* 275:4858–4864.

Balemans, W., and W. Van Hul. 2002. Extracellular regulation of BMP signaling in vertebrates: a cocktail of modulators. *Dev. Biol.* 250:231–250.

Conlon, R.A., and B.G. Herrmann. 1993. Detection of messenger RNA by in situ hybridization to postimplantation embryo whole mounts. *Methods Enzymol.* 225:373–383.

De Luca, F., K.M. Barnes, J.A. Uyeda, S. De-Levi, V. Abad, T. Palese, V. Mericq, and J. Baron. 2001. Regulation of growth plate chondrogenesis by bone morphogenetic protein-2. *Endocrinology.* 142:430–436.

Drissi, M.H., X. Li, T.J. Sheu, M.J. Zuscik, E.M. Schwarz, J.E. Puzas, R.N. Rosier, and R.J. O'Keefe. 2003. Runx2/Cbfa1 stimulation by retinoic acid is potentiated by BMP2 signaling through interaction with Smad1 on the collagen X promoter in chondrocytes. *J. Cell. Biochem.* 90:1287–1298.

Ebisawa, T., M. Fukuchi, G. Murakami, T. Chiba, K. Tanaka, T. Imamura, and K. Miyazono. 2001. Smurf1 interacts with transforming growth factor-β type I receptor through Smad7 and induces receptor degradation. *J. Biol. Chem.* 276:12477–12480.

Erlebacher, A., E.H. Filvaroff, S.E. Gitelman, and R. Derynck. 1995. Toward a molecular understanding of skeletal development. *Cell.* 80:371–378.

Flanders, K.C., E.S. Kim, and A.B. Roberts. 2001. Immunohistochemical expression of Smads 1-6 in the 15-day gestation mouse embryo: signaling by BMPs and TGF-βs. *Dev. Dyn.* 220:141–154.

Galvin, K.M., M.J. Donovan, C.A. Lynch, R.I. Meyer, R.J. Paul, J.N. Lorenz, V. Fairchild-Huntress, K.L. Dixon, J.H. Dunmore, M.A. Gimbrone, Jr., et al. 2000. A role for smad6 in development and homeostasis of the cardiovascular system. *Nat. Genet.* 24:171–174.

Haaijman, A., R.N. D'Souza, A.L. Bronckers, S.W. Goei, and E.H. Burger. 1997. OP-1 (BMP-7) affects mRNA expression of type I, II, X collagen, and matrix Gla protein in ossifying long bones in vitro. *J. Bone Miner. Res.* 12: 1815–1823.

Hanyu, A., Y. Ishidou, T. Ebisawa, T. Shimanuki, T. Imamura, and K. Miyazono. 2001. The N domain of Smad7 is essential for specific inhibition of transforming growth factor-β signaling. *J. Cell Biol.* 155:1017–1027.

Heldin, C.H., K. Miyazono, and P. ten Dijke. 1997. TGF-β signalling from cell membrane to nucleus through SMAD proteins. *Nature.* 390:465–471.

Hirota, S., A. Ito, E. Morii, A. Wanaka, M. Tohyama, Y. Kitamura, and S. Nomura. 1992. Localization of mRNA for c-kit receptor and its ligand in the brain of adult rats: an analysis using in situ hybridization histochemistry. *Brain Res. Mol. Brain Res.* 15:47–54.

Hogan, B.L. 1996. Bone morphogenetic proteins: multifunctional regulators of vertebrate development. *Genes Dev.* 10:1580–1594.

Iwasaki, S., M. Iguchi, K. Watanabe, R. Hoshino, M. Tsujimoto, and M. Kohno. 1999. Specific activation of the p38 mitogen-activated protein kinase signaling pathway and induction of neurite outgrowth in PC12 cells by bone morphogenetic protein-2. *J. Biol. Chem.* 274:26503–26510.

Jena, N., C. Martin-Seisdedos, P. McCue, and C.M. Croce. 1997. BMP7 null mutation in mice: developmental defects in skeleton, kidney, and eye. *Exp. Cell Res.* 230:28–37.

Karsenty, G., and E.F. Wagner. 2002. Reaching a genetic and molecular understanding of skeletal development. *Dev. Cell.* 2:389–406.

Kavsak, P., R.K. Rasmussen, C.G. Causing, S. Bonni, H. Zhu, G.H. Thomsen, and J.L. Wrana. 2000. Smad7 binds to Smurf2 to form an E3 ubiquitin ligase that targets the TGF β receptor for degradation. *Mol. Cell.* 6:1365–1375.

Luo, G., C. Hofmann, A.L. Bronckers, M. Sohocki, A. Bradley, and G. Karsenty. 1995. BMP-7 is an inducer of nephrogenesis, and is also required for eye development and skeletal patterning. *Genes Dev.* 9:2808–2820.

Minina, E., H.M. Wenzel, C. Kreschel, S. Karp, W. Gaffield, A.P. McMahon, and A. Vortkamp. 2001. BMP and Ihh/PTHrP signaling interact to coordinate chondrocyte proliferation and differentiation. *Development.* 128:4523–4534.

Murakami, G., T. Watabe, K. Takaoka, K. Miyazono, and T. Imamura. 2003. Cooperative inhibition of bone morphogenetic protein signaling by smurf1 and inhibitory smads. *Mol. Biol. Cell.* 14:2809–2817.

Naski, M.C., J.S. Colvin, J.D. Coffin, and D.M. Ornitz. 1998. Repression of hedgehog signaling and BMP4 expression in growth plate cartilage by fibroblast growth factor receptor 3. *Development.* 125:4977–4988.

Nishihara, A., M. Fujii, T.K. Sampath, K. Miyazono, and A.H. Reddi. 2003. Bone morphogenetic protein signaling in articular chondrocyte differentiation. *Biochem. Biophys. Res. Commun.* 301:617–622.

Olsen, B.R., A.M. Reginato, and W. Wang. 2000. Bone development. *Annu. Rev. Cell Dev. Biol.* 16:191–220.

Peters, P.W.J. 1977. Double staining of fetal skeletons for cartilage and bone. *In* Methods in Prenatal Toxicology. H.J.M.D. Neuberg and T.E. Kwasigroch, editors. Georg Thieme Verlag, Stuttgart, Germany. 153–154.

Shi, Y., and J. Massague. 2003. Mechanisms of TGF-β signaling from cell membrane to the nucleus. *Cell.* 113:685–700.

Storm, E.E., T.V. Huynh, N.G. Copeland, N.A. Jenkins, D.M. Kingsley, and S.J. Lee. 1994. Limb alterations in brachypodism mice due to mutations in a new member of the TGF β-superfamily. *Nature.* 368:639–643.

Tsumaki, N., T. Kimura, Y. Matsui, K. Nakata, and T. Ochi. 1996. Separable cis-regulatory elements that contribute to tissue- and site-specific α2(XI) collagen gene expression in the embryonic mouse cartilage. *J. Cell Biol.* 134: 1573–1582.

Tsumaki, N., K. Tanaka, E. Arikawa-Hirasawa, T. Nakase, T. Kimura, J.T. Thomas, T. Ochi, F.P. Luyten, and Y. Yamada. 1999. Role of CDMP-1 in skeletal morphogenesis: promotion of mesenchymal cell recruitment and chondrocyte differentiation. *J. Cell Biol.* 144:161–173.

Tsumaki, N., T. Nakase, T. Miyaji, M. Kakiuchi, T. Kimura, T. Ochi, and H. Yoshikawa. 2002. Bone morphogenetic protein signals are required for cartilage formation and differently regulate joint development during skeletogenesis. *J. Bone Miner. Res.* 17:898–906.

Valcourt, U., J. Gouttenoire, A. Moustakas, D. Herbage, and F. Mallein-Gerin. 2002. Functions of transforming growth factor-β family type I receptors and Smad proteins in the hypertrophic maturation and osteoblastic differentiation of chondrocytes. *J. Biol. Chem.* 277:33545–33558.

Volk, S.W., P. Luvalle, T. Leask, and P.S. Leboy. 1998. A BMP responsive transcriptional region in the chicken type X collagen gene. *J. Bone Miner. Res.* 13:1521–1529.

Yi, S.E., A. Daluiski, R. Pederson, V. Rosen, and K.M. Lyons. 2000. The type I BMP receptor BMPRIB is required for chondrogenesis in the mouse limb. *Development.* 127:621–630.

Zhang, Y., C. Chang, D.J. Gehling, A. Hemmati-Brivanlou, and R. Derynck. 2001. Regulation of Smad degradation and activity by Smurf2, an E3 ubiquitin ligase. *Proc. Natl. Acad. Sci. USA.* 98:974–979.

Zhu, H., P. Kavsak, S. Abdollah, J.L. Wrana, and G.H. Thomsen. 1999. A SMAD ubiquitin ligase targets the BMP pathway and affects embryonic pattern formation. *Nature.* 400:687–693.

J Bone Miner Metab (2004) 22:346–351
DOI 10.1007/s00774-003-0493-8

Journal of
Bone and
Mineral
Metabolism

Localization of RANKL in osteolytic tissue around a loosened joint prosthesis

Mitsuru Horiki, Takanobu Nakase, Akira Myoui, Nobuhiko Sugano, Takashi Nishii, Tetsuya Tomita, Takahiro Miyaji, and Hideki Yoshikawa

Department of Orthopaedic Surgery, Osaka University Graduate School of Medicine (E3), 2-2 Yamadaoka, Suita 565-0871, Japan

Abstract Osteoclastogenesis is a key event of the cellular reaction in prosthetic loosening. Immunohistochemistry and reverse transcription-polymerase chain reaction (RT-PCR) were used to study the localization and expression of receptor activator of nuclear factor kappa B ligand (RANKL), a potent factor for osteoclastogenesis in the membranous tissue formed around loosened prosthetic joint implants. RANKL was identified in a wide variety of cells appearing in this membranous tissue. At least three types of RANKL-positive cells were identified, including prolyl 4-hydroxylase (PH)-positive fibroblast lineage cells, CD68 cells, and tartrate-resistant acid phosphatase (TRAP)-positive mononuclear and multinucleated macrophage lineage cells. Tumor necrosis factor (TNF)-alpha-converting enzyme (TACE) was colocalized with *RANKL* in these cells, suggesting the in-situ release of this factor. RT-PCR confirmed the actual expression of the *RANKL* and *TACE* genes in the tissues around the loosened implant. These observational findings indicate the possible synthesis of RANKL by fibroblast and macrophage lineage cells, and suggest the in-situ involvement of RANKL in both osteoclastogenesis and osteoclastic bone resorptive events occurring in prosthetic joint loosening.

Key words loosening · RANKL · TACE

Introduction

The mechanism of cellular reaction to artificially implanted materials is a major concern for orthopedic surgeons. Cellular events occurring around implanted materials sometimes cause aseptic loosening of the implant, leading to serious clinical problems [1,2]. Osteolysis caused by osteoclastic bone resorption is reportedly a key event in the mechanism of loosening, and several factors have been demonstrated to be involved in this mechanism [3–6].

Recently, a potent molecule responsible for osteoclastogenesis, has been identified as a ligand for receptor activation of nuclear factor (NF)-κB (RANKL) [7–9]. RANKL is a membrane-bound 40- to 45-kDa protein that is a member of the tumor necrosis factor (TNF) family. Together with macrophage colony-stimulating factor (M-CSF), RANKL has been shown to support the differentiation and maturation of osteoclasts sin vitro in mouse, rat, and human cells. Mice with a disrupted *RANKL* gene exhibited an osteopetrotic phenotype, suggesting that RANKL plays an essential role in osteoclastic bone resorption [9].

Based on this knowledge, it appears that RANKL may be a candidate molecule responsible for the cellular events leading to prosthesis loosening. RANKL appears to be expressed and produced by cells derived from membranous tissues located adjacent to loosened implants, suggesting that RANKL may be a targeting molecule that regulates the osteolytic events occurring in prosthetic loosening. However, little is known about either the in-situ localization of RANKL or the cell types expressing RANKL in human prosthetic loosening.

The purpose of this study was to elucidate the involvement of RANKL in the cellular mechanism of the osteolytic reaction occurring in the loosened prosthesis. The expression and localization of RANKL in the tissue surrounding the loosened prosthesis were examined by reverse transcription-polymerase chain reaction (RT-PCR) and immunohistochemistry, respectively. In addition, the expression and localization of TNF-alpha converting enzyme (TACE) (shown to cleave RANKL and release its soluble form) were also examined.

Offprint requests to: M. Horiki
(e-mail: horiki@ort.med.osaka-u.ac.jp)
Received: August 12, 2003 / Accepted: November 12, 2003

Patients and methods

Patients

Tissue samples were obtained during surgery from five patients who underwent revision total hip arthroplasty. Written informed consent was obtained from all patients. All samples were taken from the membranous tissue formed around loosened prosthetic joint implants. In all patients, radiographic and clinical findings indicated aseptic loosening with osteolysis. Occult pyogenic infection was excluded by general clinical examination, full blood count, C-reactive protein levels, and intraoperative macroscopic findings. Duration of implant (i.e., the time from primary surgery to revision surgery) ranged from 6 to 32 years. A summary of patient information is presented in Table 1.

Preparation of tissues

Tissue samples were prepared as previously described [10]. They were fixed in 4% paraformaldehide (Merck KGaA, Darmstadt, Germany) in phosphate-buffered saline (PBS; pH 7.4) (Sigma Chemical, St. Louis, MO, USA), dehydrated in an ethanol series, and embedded in paraffin. Sections 5-μm were made on a microtome, and some sections were stained with hematoxylin and eosin. The remaining serial sections were prepared for immunohistochemistry.

Immunohistochemistry

Immunohistochemistry was performed using the streptavidin-peroxidase method, with histofine SAB-PO kits (Nichirei, Tokyo, Japan) according to the method recommended by the manufacturer [11]. Three different antibodies were used as primary antibodies: (1) mouse polyclonal antibody against human CD68 (purchased from Dako, Santa Barbara, CA, USA; 1:200 dilution); (2) goat polyclonal antibody against human RANKL (purchased from Santa Cruz Biotechnology, Santa Cruz, CA, USA; 1:200 dilution); and (3) mouse monoclonal antibody against human prolyl 4-hydroxylase (PH; purchased from Daiichi Fine Chemical, Tokyo, Japan; 1:400 dilution); we also used a rabbit polyclonal antibody against human TACE (purchased from R&D Systems, Minnesota, MN, USA). Tissue sections were briefly deparaffinized, dehydrated, and placed in 3% H_2O_2 in methanol to block endogenous peroxidase. After a washing in PBS (pH 7.2), the sections were blocked with 10% normal serum of the same species as the secondary antibody to minimize background staining, followed by incubation with the primary antibody for 2h at room temperature. Normal serum of the same species as the primary antibody was used as a control for the primary antibody. After a washing in PBS, the sections were incubated with the secondary antibody (rabbit Ig-G: Nichirei, Tokyo, Japan) for 20min at room temperature in a humid chamber, and then incubated with peroxidase-conjugated streptavidin (Nichirei) for 20min at room temperature in a humid chamber and washed in PBS. Finally, color reaction was performed using the substrate reagent 3,3′ diaminobenzidine tetrahydrochloride (Dojindo, Tokyo, Japan). Sections were counterstained with hematoxylin and mounted.

Tartrate-resistant acid phosphatase (TRAP) staining was performed, using a TRAP staining kit (Sigma, St. Louis, MO, USA). TRAP activity was detected according to a procedure using naphthol AS-TR phosphate containing 10mM L(+)- tartaric acid as substrate. These sections were also counterstained with hematoxylin.

RNA extraction and RT-PCR

Total RNA was extracted from the fibrous tissues of the five patients by an acid guanidine thiocyanate-phenol-chloroform (AGPC) method, using Trizol (Gibco, Grand Island, NY, USA) according to the manufacturer's instructions. In 1 μg of tRNA from each sample genomic DNA was eliminated with DNaseI (Takara, Japan) and tRNA was reverse transcribed in 20 μl of a reaction mixture containing 200 U of SuperScript II reverse transcriptase (Gibco) and 0.5 μg Oligo$(dT)_{12-18}$ primer (Gibco). Subsequently, 1 μl of each reaction product was amplified in 25 μl of a PCR mixture containing 0.125 U of Taq DNA polymerase and 12.5 pmol each of primers (sense and antisense). Oligonucleotides

Table 1. Summary of patients with loosened components

Case no.	Age at revision surgery (years)	Sex	Duration of implant (years)	Location of tissue
1	52	Male	32	Femoral
2	54	Male	6	Femoral
3	77	Female	16	Acetabular
4	83	Female	19	Femoral and acetabular
5	60	Female	12	Femoral and acetabular

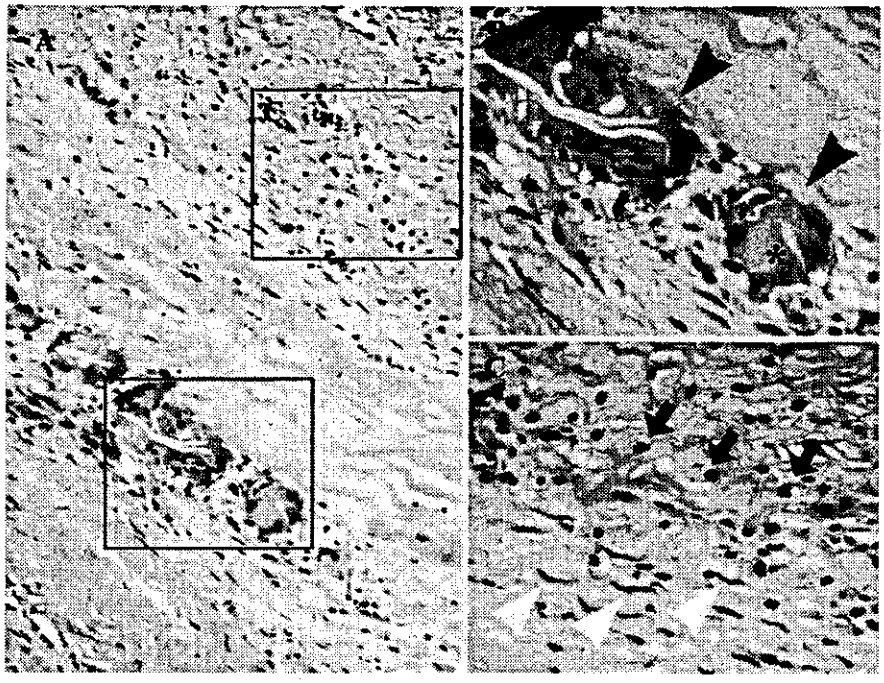

Fig. 1. Representative photomicrographs of fibrogranulomatous tissue retrieved at the time of revision surgery for aseptic prosthesis loosening with osteolysis. **A** is the low power view in the fibrogranulomatous tissue. **B** and **C** are higher power views of *upper* and *lower boxed areas* in **A** respectively. **C** shows mononuclear round cells (*arrows*); **B** shows multinucleated giant cells (*black arrowheads*), and **C** also shows fibroblastic cells (*white arrowheads*). Note wear particle surrounded by multinucleated giant cells (*asterisk* in **B**). Paraffin-embedded section was stained with H&E by conventional methods. **A** ×200; **B** ×400; **C** ×400

used for the reverse transcription and PCR were as follows; human RANKL: 5′-AAATCCCAAGTTCT CATACCC -3′ (5′ sense), 5′-CCCACTGGCAGGT AAATACGC -3′ (3′ antisense) (base numbers 871–891 and 1239–1259, respectively; Gene bank accession no. AF19047), human TACE: 5′-ACCTGAAGAGCTTG TTCATCGAG-3′ (5′ sense) and 5′-CCATGAAGTGT TCCGATAGATGTC-3′ (3′ antisense) (base numbers 776–798 and 927–950, respectively; GenBank accession no. XM015606). Thirty-five cycles were performed with an iCycler Thermal Cycler (Bio-Rad, USA), at 94°C for 0.5 min, 60°C for 0.5 min, 72°C for 1 min, then at 72°C for 7 min at the end of the procedure. A 317-bp fragment of human β-actin was also amplified as a control. Ten-microliter aliquots of the PCR products were electrophoresed in an agarose gel.

Results

Histology and immunohistochemistry

Morphologically, at least three types of cells, i.e., macrophage-like mononuclear cells (Fig. 1C, black arrows), multinucleated giant cells (Fig. 1B, black arrowheads), and fibroblast-like cells (Fig. 1C, white arrowheads) were observed in the membranous tissues surrounding the loosened prosthesis obtained from five patients during revision surgery (Fig. 1A). In the specimens from all patients, the tissues also contained many small clear particles that glowed under polarized light; these were thought to be polyethylene wear particles (Fig. 1B, asterisk). In only one case, metal particles were contained in the tissue. Almost all the multinucleated giant cells had phagocytosed these polyethylene wear particles. These cells looked morphologically similar to foreign-body giant cells in soft-tissue foreign-body granuloma. Both the mononuclear and the multinucleated giant cells showed positive immunoreactivity for CD68 (macrophage-associated antigen; Fig. 2A,E). Most of the CD68-positive cells were also positive for TRAP, which is a marker for cells of the osteoclast lineage (Fig. 2D,H). These CD68- and TRAP-positive cells showed positive immunoreactivity for RANKL (Fig. 2B,F) and TACE (Fig. 2C,G). Not only polyethylene particle-phagocytosed cells but also non-phagocytosed cells showed positive immunoreactivity for anti-RANKL and anti-TACE antibody. The degrees of immunoreactivity for anti-RANKL and anti-TACE antibody showed no difference between polyethylene particle-phagocytosed cells and non-phagocytosed cells. Fibroblast-like cells were positively immunostained by anti-PH antibody (Fig. 3A), anti-RANKL antibody (Fig. 3B), and anti-TACE antibody (Fig. 3C), but were negative for CD68 (Fig. 3D) and negative for TRAP (data not shown). These findings were observed in all cases examined.

Expression of RANKL and TACE mRNA determined by RT-PCR

In all cases, we detected RANKL and TACE mRNAs by RT-PCR as single bands at the expected molecular

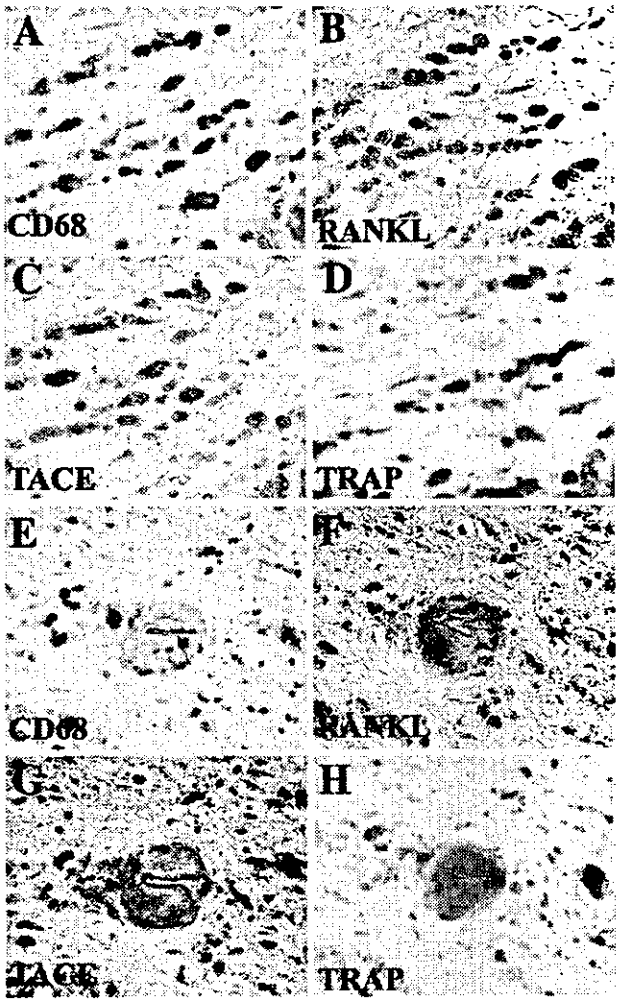

Fig. 2. Immunohistochemical staining (**A–C**, **E–G**), and tartrate-resistant acid phosphatase (*TRAP*) staining (**D** and **H**) were carried out on serial sections, as described in "Patients and methods", using a monoclonal antibody against human CD68 (**A** and **E**), a polyclonal antibody against human receptor actwater of nuclear factor κB ligand (*RANKL*; **B**, and **F**), and a polyclonal antibody against human tumor necrosis factor-alpha-converting enzyme (*TACE*; **C**, and **G**). CD68- and TRAP-positive mononuclear round cells and multinucleated giant cells were positive for TACE and RANKL. The sections were counterstained with hematoxylin. **A–H**, ×400

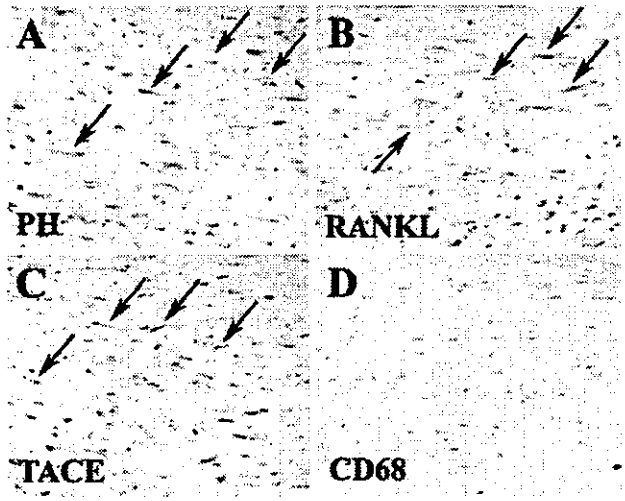

Fig. 3. Immunohistochemical staining (**A–D**) was carried out on serial sections as described in "Patients and methods", using a monoclonal antibody against human prolyl 4-hydroxyase (*PH*; **A**), a polyclonal antibody against human RANKL (**B**), a polyclonal antibody against human TACE (**C**), and a monoclonal antibody against human CD68 (**D**). PH-positive fibroblast-like cells were positive for TACE and RANKL (*arrows*), and negative for CD68 and TRAP (data not shown). The sections were counterstained with hematoxylin. **A–D**, ×400

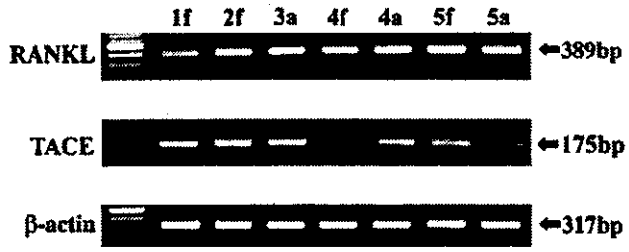

Fig. 4. Detection of RANKL and TACE mRNA, using reverse transcription polymerase chain reaction (RT-PCR) analysis. RT-PCR products from five patients (*lanes 1–5*; cases 1–5; *a*, obtained from around acetabular implant; *f*, obtained from around femoral implant) were detected by electrophoresis on a 2% agarose gel, as described in "Patients and methods". RANKL and TACE mRNAs were detected in all five cases. B-actin mRNA expression was also examined by RT-PCR as an internal reference

weights for human RANKL and TACE (Fig. 4). Sequencing analysis confirmed that the product was identical to RANKL and TACE.

Discussion

Our findings demonstrate the immunolocalization of RANKL in cells of the tissues surrounding a loosened prosthesis. To the best of our knowledge, this is the first description regarding the in-situ localization of RANKL in the tissues around a loosened prosthesis in humans. RANKL mRNA was identified by RT-PCR, supporting the immunohistochemical localization. The present findings demonstrated the colocalization of TACE and RANKL, indicating the possible release of RANKL protein in the membranous tissue surrounding a loosened prosthesis. However, the precise cellular mechanisms responsible for the regulation of the syn-

thesis and release of this key molecule need further investigation.

TACE belongs to the adamalysin family of zinc-dependent metalloproteinases. It plays a role in the shedding of membrane-bound interleukin (IL)-6 receptor (R) and TNF-α [12, 13]. TNF-α, IL-6, and IL-6R have been identified in the membranous tissue surrounding a loosened prosthesis by immunohistochemistry and RT-PCR [4, 14, 15]. Together with the reported key roles of these cytokines in the mechanism of osteoclastic bone resorption [16], TACE may contribute to the shedding of TNF-α, and IL-6R, leading to the acceleration of osteoclastic bone resorption in the microenviroment of prosthetic loosening.

Recent studies have revealed the clinical significance of RANKL in osteolytic conditions. These studies detected RANKL mRNA in fibrous tissues associated with prosthetic loosening, but did not identify the cell types producing RANKL in vivo [17, 18]. Our study findings confirm the original observations, as well as identifying the cell types expressing RANKL. In our histological examinations, RANKL was expressed by at least three distinct types of cells: CD68/TRAP-positive mononuclear histiocytic cells, CD68/TRAP-positive multinucleated giant cells, and PH-positive fibroblast-like cells. In osteoclastogenesis, RANKL was initially reported to be expressed by stromal fibroblastic cells, but not by macrophage-lineage cells [19]. Studies of pathological conditions have demonstrated that RANKL is expressed by TRAP-positive osteoclast-like cells in rheumatoid arthritis [20] and in bone-resorbing osteoclast-like cells in giant-cell bone tumors [21]. Very recent work has revealed that particle-activated cells of monocyte/macrophage lineage are capable of producing RANKL in vitro [17]. RANKL seems likely to be synthesized by macrophage/monocyte/osteoclast lineage cells under pathological conditions, rather than in the normal physiological state of bone remodeling.

In other recent work, RANKL has been demonstrated to activate and promote particle-induced osteoclastogenesis in vitro [22], while CD68-positive mono/multinucleated cells, isolated from osteolytic fibrous tissues associated with total hip replacement, were earlier reported to be capable of bone resorption in vitro [23]. In conjunction with these previous in vitro findings, our present in-situ immunohistochemical findings suggest the possible contribution of fibroblast lineage cells and macrophage lineage cells to osteoclastogenesis and osteoclastic bone resorption via RANKL, in the mechanism of prosthetic loosening.

The possible involvement of RANKL synthesized by fibroblast- and macrophage-lineage cells in the mechanism of prosthetic loosening suggests that RANKL, as well as fibroblast- and macrophage-lineage cells, may be a target for efforts to prevent such loosening. In fact, it has recently been reported that antagonization of RANKL successfully inhibited osteolysis in animal models of activated osteoclastic bone resorption [24–31]. Although current findings are still quite preliminary, further studies regarding the in vivo action of RANKL in the mechanism of prosthetic loosening should be addressed. A novel therapy targeting RANKL in both fibroblastic and macrophage-lineage cells could lead to the prevention of aseptic prosthesis loosening after joint replacement surgery, a major concern for orthopedic surgeons.

Acknowledgments. This work was partly supported by grants from the Ministry of Education, Culture, Sports, Science, and Technology of Japan and the New Energy and Industrial Technology Development Organization. We thank Miss Kanae Asai for her technical assistance in the preparation of histological sections.

References

1. Paterson M, Fulford P, Denham R (1986) Loosening of the femoral component after total hip replacement. The thin black line and the sinking hip. J Bone Joint Surg Br 68:392–397
2. Harris WH (1994) Osteolysis and particle disease in hip replacement. A review. Acta Orthop Scand 65:113–123
3. Atkins RM, Langkamer VG, Perry MJ, Elson CJ, Collins CM (1997) Bone-membrane interface in aseptic loosening of total joint arthroplasties. J Arthroplasty 12:461–464
4. Goodman SB, Huie P, Song Y, Schurman D, Maloney W, Woolson S, Sibley R (1998) Cellular profile and cytokine production at prosthetic interfaces. Study of tissues retrieved from revised hip and knee replacements. J Bone Joint Surg Br 80:531–539
5. Jones LC, Frondoza C, Hungerford DS (1999) Immunohistochemical evaluation of interface membranes from failed cemented and uncemented acetabular components. J Biomed Mater Res 48:889–898
6. Voronov I, Santerre JP, Hinek A, Callahan JW, Sandhu J, Boynton EL (1998) Macrophage phagocytosis of polyethylene particulate in vitro. J Biomed Mater Res 39:40–51
7. Anderson DM, Maraskovsky E, Billingsley WL, Dougall WC, Tometsko ME, Roux ER, Teepe MC, DuBose RF, Cosman D, Galibert L (1997) A homologue of the TNF receptor and its ligand enhance T-cell growth and dendritic-cell function. Nature 390:175–179
8. Horowitz MC, Xi Y, Wilson K, Kacena MA (2001) Control of osteoclastogenesis and bone resorption by members of the TNF family of receptors and ligands. Cytokine Growth Factor Rev 12:9–18
9. Kong YY, Feige U, Sarosi I, Bolon B, Tafuri A, et al. (1999) Activated T cells regulate bone loss and joint destruction in adjuvant arthritis through osteoprotegerin ligand. Nature 402:304–309
10. Nakase T, Kaneko M, Tomita T, Myoui A, Ariga K, Sugamoto K, Uchiyama Y, Ochi T, Yoshikawa H (2000) Immunohistochemical detection of cathepsin D, K, and L in the process of endochondral ossification in the human. Histochem Cell Biol 114:21–27
11. Ohsawa Y, Nitatori T, Higuchi S, Kominami E, Uchiyama Y (1993) Lysosomal cysteine and aspartic proteinases, acid phosphatase, and an endogenous cysteine proteinase inhibitor, cystatin-beta, in rat osteoclasts. J Histochem Cytochem 41:1075–1083
12. Black RA, Rauch CT, Kozlosky CJ, Peschon JJ, Slack JL, et al. (1997) A metalloproteinase disintegrin that releases tumour-necrosis factor-alpha from cells. Nature 385:729–733

13. Matthews V, Schuster B, Schutze S, Bussmeyer I, Ludwig A, Hundhausen C, Sadowski T, Saftig P, Hartmann D, Kallen KJ, Rose-John S (2003) Cellular cholesterol depletion triggers shedding of the human interleukin-6 receptor by ADAM10 and ADAM17 (TACE). J Biol Chem 278:38829–38839
14. Neale SD, Athanasou NA (1999) Cytokine receptor profile of arthroplasty macrophages, foreign body giant cells and mature osteoclasts. Acta Orthop Scand 70:452–458
15. Jones LC, Frondoza C, Hungerford DS (1999) Immunohistochemical evaluation of interface membranes from failed cemented and uncemented acetabular components. J Biomed Mater Res 48:889–898
16. Sugiyama T (2001) Involvement of interleukin-6 and prostaglandin E2 in periarticular osteoporosis of postmenopausal women with rheumatoid arthritis. J Bone Miner Metab 19:89–96
17. Haynes DR, Crotti TN, Potter AE, Loric M, Atkins GJ, Howie DW, Findlay DM (2001) The osteoclastogenic molecules RANKL and RANK are associated with periprosthetic osteolysis. J Bone Joint Surg Br 83:902–911
18. Sabokbar A, Pocock A, Kudo O, Neale SD, Schulze E, Danks L, Athanasou NA (2001) Exression of osteoclastgenic markers in inflamed synovial tissues in prosthesis loosening and arthritis. Bone 28:S163
19. Takahashi N, Udagawa N, Suda T (1999) A new member of tumor necrosis factor ligand family, ODF/OPGL/TRANCE/RANKL, regulates osteoclast differentiation and function. Biochem Biophys Res Commun 256:449–455
20. Romas E, Bakharevski O, Hards DK, Romas E, Bakharevski O, Hards DK, Kartsogiannis V, Quinn JM, Ryan PF, Martin TJ, Gillespie MT (2000) Expression of osteoclast differentiation factor at sites of bone erosion in collagen-induced arthritis. Arthritis Rheum 43:821–826
21. Atkins GJ, Haynes DR, Graves SE, Evdokiou A, Hay S, Bouralexis S, Findlay DM (2000) Expression of osteoclast differentiation signals by stromal elements of giant cell tumors. J Bone Miner Res 15:640–649
22. Greenfield EM, Bi Y, Ragab AA, Goldberg VM, Van De Motter RR (2002) The role of osteoclast differentiation in aseptic loosening. J Orthop Res 20:1–8
23. Athanasou NA, Quinn J, Bulstrode CJ (1992) Resorption of bone by inflammatory cells derived from the joint capsule of hip arthroplasties. J Bone Joint Surg Br 74:57–62
24. Atkins GJ, Bouralexis S, Haynes DR, Graves SE, Geary SM, Evdokiou A, Zannettino AC, Hay S, Findlay DM (2001) Osteoprotegerin inhibits osteoclast formation and bone resorbing activity in giant cell tumors of bone. Bone 28:370–377
25. Croucher PI, Shipman CM, Lippitt J, Perry M, Asosingh K, Hijzen A, Brabbs AC, Van Beek EJ, Holen I, Skerry TM, Dunstan CR, Russell GR, Van Camp B, Vanderkerken K (2001) Osteoprotegerin inhibits the development of osteolytic bone disease in multiple myeloma. Blood 98:3534–3540
26. Min H, Morony S, Sarosi I, Dunstan CR, Capparelli C, Scully S, Van G, Kaufman S, Kostenuik PJ, Lacey DL, Boyle WJ, Simonet WS (2000) Osteoprotegerin reverses osteoporosis by inhibiting endosteal osteoclasts and prevents vascular calcification by blocking a process resembling osteoclastogenesis. J Exp Med 192:463–474
27. Oyajobi BO, Anderson DM, Traianedes K, Williams PJ, Yoneda T, Mundy GR (2001) Therapeutic efficacy of a soluble receptor activator of nuclear factor kappaB-IgG Fc fusion protein in suppressing bone resorption and hypercalcemia in a model of humoral hypercalcemia of malignancy. Cancer Res 61:2572–2578
28. Simonet WS, Lacey DL, Dunstan CR, Simonet WS, Lacey DL, et al. (1997) Osteoprotegerin: a novel secreted protein involved in the regulation of bone density. Cell 89:309–319
29. Ulrich-Vinther M, Carmody EE, Goater JJ, Soballe K, O'Keefe RJ, Schwarz EM (2002) Recombinant adeno-associated virus-mediated osteoprotegerin gene therapy inhibits wear debris-induced osteolysis. J Bone Joint Surg Am 84:1405–1412
30. Goater JJ, O'Keefe RJ, Rosier RN, Puzas JE, Schwarz EM (2002) Efficacy of ex vivo OPG gene therapy in preventing wear debris induced osteolysis. J Orthop Res 20:169–173
31. Juji T, Hertz M, Aoki K, Horie D, Ohya K, Gautam A, Mouritsen S, Oda H, Nakamura K, Tanaka S (2002) A novel therapeutic vaccine approach, targeting RANKL, prevents bone destruction in bone-related disorders. J Bone Miner Metab 20: 266–268

TISSUE ENGINEERING
Volume 10, Number 5/6, 2004

Capillary Vessel Network Integration by Inserting a Vascular Pedicle Enhances Bone Formation in Tissue-Engineered Bone Using Interconnected Porous Hydroxyapatite Ceramics

SHOSUKE AKITA, M.D.,[1,2] NORIYUKI TAMAI, M.D.,[1] AKIRA MYOUI, M.D.,[1] MASATAKA NISHIKAWA, M.D.,[1] TAKASHI KAITO, M.D.,[1] KUNIO TAKAOKA, M.D.,[3] and HIDEKI YOSHIKAWA, M.D.[1]

ABSTRACT

The aim of the present study was to investigate the possibility of integrating porous hydroxyapatite (HA) ceramics with a capillary vessel network via insertion of a vascular pedicle, and to determine whether this procedure enhances new bone formation in tissue engineering of bone. First, synthetic interconnected porous HA (IP-CHA) was implanted subcutaneously into rat groin with or without insertion of superficial inferior epigastric vessels. At 6 weeks, IP-CHA with vascular insertion contained thick fibrous connective tissue with a number of large blood vessels that seemed to derive from the inserted vascular bundle. Next, IP-CHA loaded with recombinant human bone morphogenetic protein 2 (BMP, 2 or 10 μg/block) was implanted with or without vascular insertion. At 3 weeks, IP-CHA/BMP (10 μg) composite with vascular insertion exhibited abundant new bone formation in the pores of the deep portion close to the inserted vessels. In contrast, IP-CHA/BMP (10 μg) without vascular insertion showed poor bone formation. Histomorphometric analysis demonstrated that vascular insertion significantly increased new bone formation. In IP-CHAs with a lower dose of BMP (2 μg), no bone formation was found, with or without vascular insertion. These results suggest that the present system of integrating a vascular network with IP-CHA is a useful technique for bone tissue engineering.

INTRODUCTION

WITH ADVANCES in materials technology, many kinds of biocompatible biomaterials have been used clinically for the treatment of bone defects. Hydroxyapatite (HA) ceramics are widely used because of their good osteoconductivity.[1–5] However, use of HA ceramics as bone substitute is still limited, and is not applicable to conditions such as large bone defects and avascularity, because blood supply is essential for new bone formation.[6–8] Currently, vascularized autogenous bone grafting is a standard technique for such cases because of its superior osteogenic potential, which is probably due to its abundant blood supply.[9,10] However, this technique has considerable disadvantages, including donor site morbidity and limited availability.

Meanwhile, interest in tissue-engineering techniques has been increasing and there have been several experimental studies of bone engineering based on stem cell technology or osteoinductive molecules such as bone morphogenetic protein 2 (BMP-2) and osteogenic protein 1 (OP-1). However, there have been few studies of clin-

[1]Department of Orthopedics, Osaka University Graduate School of Medicine, Suita, Japan.
[2]Department of Orthopedic Surgery, Hoshigaoka Koseinenkin Hospital, Osaka, Japan.
[3]Department of Orthopedic Surgery, Osaka City University Medical School, Osaka, Japan.

ical results of the use of tissue-engineered bone,[11] and it is reasonable to assume that clinical application of this technique would be limited by the problem of blood supply.

We developed novel HA ceramics with an interconnected porous structure (IP-CHA) that allows cells and tissues to penetrate deep into the pores.[12] By inserting a vascular bundle into a block of IP-CHA, a block can be prefabricated with a vascular network in its interconnected pores derived from the inserted vessels. We hypothesized that, when applied to tissue engineering of bone, these blocks would enhance new bone formation because of their improved blood supply. The aim of the present study was to investigate the possibility of integrating a vascular network with interconnected porous HA via insertion of a vascular bundle, and to determine whether use of this technique with IP-CHA and recombinant human BMP 2 (rhBMP-2) enhances bone formation in tissue-engineered bone.

MATERIALS AND METHODS

Animals and materials

Male Sprague-Dawley rats (age, 12 weeks; average weight, 250 g) were purchased from Oriental Yeast (Tokyo, Japan). All animals were kept in the Institute of Experimental Animal Science, Osaka University Medical School, and all experiments were conducted according to the institute's *Guidelines for the Care and Use of Laboratory Animals.* IP-CHA (porosity, 75%; average pore diameter, 150 μm; average interpore connection diameter, 40 μm) was donated by Toshiba Ceramics (Tokyo, Japan) and MMT (Osaka, Japan). rhBMP-2 and poly-D, L-lactic acid-*p*-dioxanone polyethylene glycol copolymer (PLA-DX-PEG) were donated by Yamanouchi Pharmaceutical (Tokyo, Japan) and Taki Chemical (Kakogawa, Japan), respectively. Anti-von Willbrand factor antibody was purchased from Dako Japan (Kyoto, Japan).

Preparation of interconnected porous HA ceramic implants

Cylindrical IP-CHA blocks (diameter, 6 mm; length, 10 mm) were prepared as described previously.[12] A longitudinal drill hole (diameter, 1.5 mm) was made along the central axis of each IP-CHA block. For the experiments concerning tissue engineering of bone, IP-CHA blocks were loaded with rhBMP-2 (2 μg/block or 10 μg/block) and the synthetic biodegradable polymer PLA-DX-PEG (20 mg/block; carrier for BMP-2).[13]

Establishment of an IP-CHA/vascular pedicle insertion model

Rats were anesthetized and kept in a supine position. A diagonal incision was made along the femoral vessels of the right leg, and the superficial inferior epigastric vessels were identified. A ligation amputation was performed at the distal end close to the junction with the superficial femoral vessels, and the surrounding connective tissue was then scraped off to mobilize the vessels as a pedicle.

Six vascularized IP-CHA blocks were constructed. The superficial inferior epigastric vessels were inserted into the drill hole of an IP-CHA block. The block was then wrapped in polyethylene filter membrane (Isopore; pore size, 0.4 μm; Millipore, Bedford, MA), in order to avoid penetration by new blood vessels from the surrounding area. Each of the six vascularized IP-CHA blocks was then implanted into a subcutaneous pocket made in the groin of a rat. These six rats comprised the vascularized IP-CHA group.

Six control (nonvascularized) IP-CHA blocks were constructed according to the above-described procedure, except that this time nothing was inserted into the drill hole of the block. These six rats comprised the control IP-CHA group.

Development of vascular network in the pores of IP-CHA

Six weeks after surgery, the groin incision was reopened under anesthesia, and the filter membrane was removed. In three animals from each of the two groups (vascularized group and control group), a new incision was made in the chest, and 10 mL of India ink was inoculated into the left ventricle of the heart. After India ink perfusion was complete, the implant surface was carefully examined for black stains. The IP-CHA block was

FIG. 1. Insertion of vascular bundle into IP-CHA. Gross appearance of superficial inferior epigastric vessels (arrowhead) inserted into the IP-CHA block. Six weeks after implantation, firm arterial pulsation was observed at the entrance of the block.

then carefully removed and prepared for microscopic examination of ink perfusjon on undecalcified sections. All other specimens were harvested and fixed in 4% paraformaldehyde (pH 7.4) at 4°C for 24 h.

Tissue engineering of bone using IP-CHA integrated with vascular bundle

In the second set of experiments, we investigated whether vascular bundle insertion enhances new bone

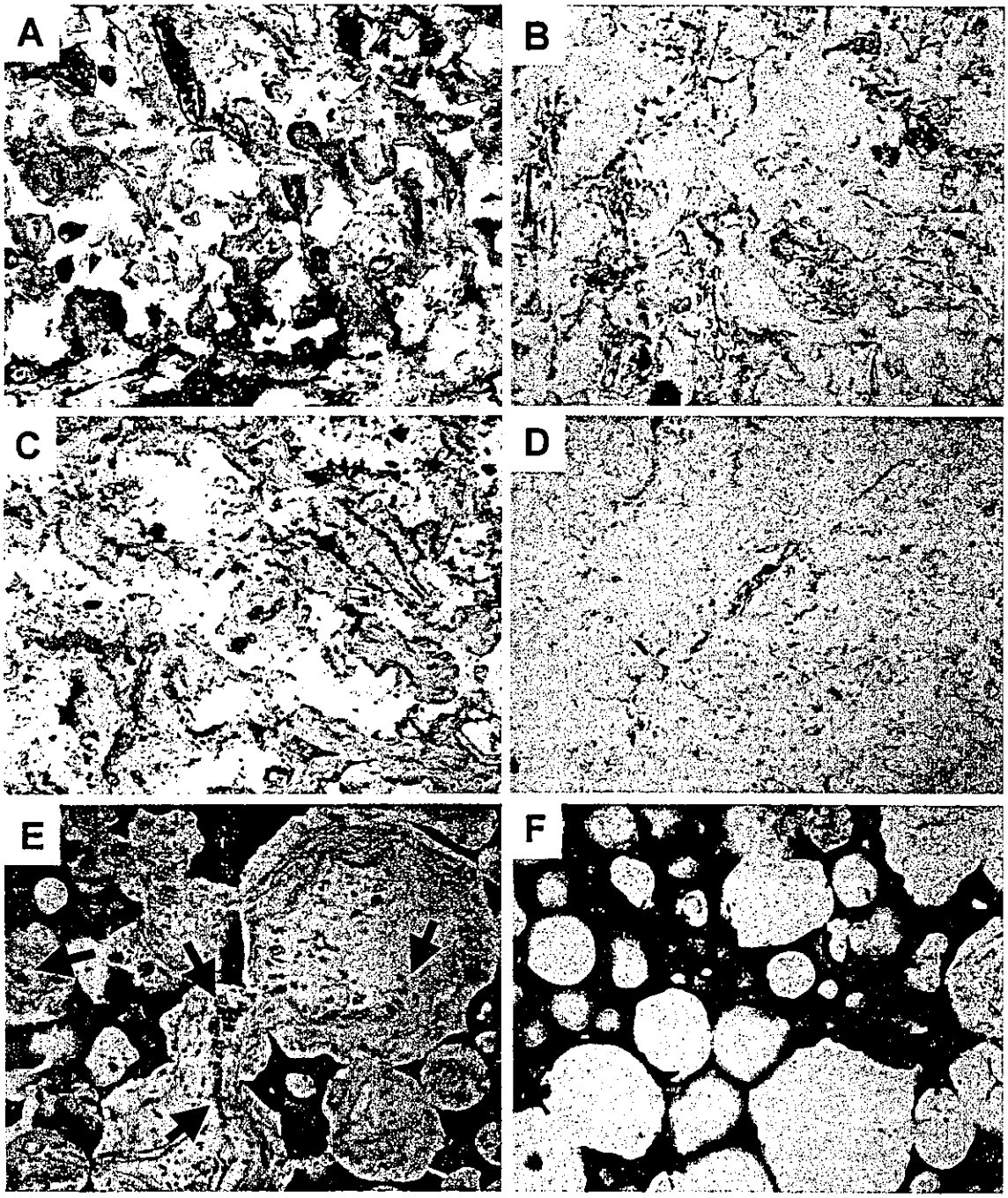

FIG. 2. Representative photomicrographs of IP-CHA 6 weeks after subcutaneous implantation with (**A**, **C**, and **E**) or without (**B**, **D**, and **F**) vascular bundle insertion. (**A** and **B**) Hematoxylin and eosin-stained sections (original magnification, ×100). (**A**) In IP-CHA with vascular bundle insertion, many thick blood vessels accompanied by active fibrous connective tissue formation were observed in the pores. (**B**) In the control IP-CHA group, loose fibrous tissues with microvessels were seen in the pores close to the peripheral surface of the block, but not in the deep pores. (**C** and **D**) Immunostaining for von Willebrand factor (original magnification, ×100). Note abundant thick vessels in IP-CHA with vascular bundle insertion (**C**). (**E** and **F**) Toluidine blue staining of hard tissue sections after India ink perfusion. In IP-CHA with vascular bundle insertion, thick blood vessels containing India ink were observed (**E**, arrows).

formation in tissue-engineered bone. The four rats in the vascularized BMP/IP-CHA group received an IP-CHA implant with vascular insertion loaded with 10 μg of rhBMP-2. The four rats in the control BMP/IP-CHA group were implanted with an IP-CHA block without vascular insertion loaded with 10 μg of rhBMP-2. Similarly, 10 rats were implanted with an IP-CHA block loaded with 2 μg of rhBMP-2: 5 rats with vascular insertion, and 5 rats without vascular insertion. Three weeks after implantation, all implants were removed and prepared for histological examination.

Histological examination

For undecalcified sections, tissue samples were fixed in 70% ethanol for 48 h, dehydrated, and then embedded in polymethyl methacrylate. Sections (6 μm thick) along the drill hole were then made, and were stained with toluidine blue for assessment of histological details.

All other tissue samples were decalcified in 20% EDTA (pH 7.4) at 4°C, dehydrated, and then embedded in paraffin. Each sample was cut into 5 μm sections along the drill hole; these were processed for further study. Hematoxylin–eosin staining was used to examine details of tissue in the pores. To visualize vessels in the pores, immunohistochemical staining using anti-von Willebrand factor antibody was performed as described previously.[14]

Quantification of bone formation in the pores

For quantitative assessment of bone formation in the pores of BMP/IP-CHA implants, the hematoxylin–eosin-stained cross-section of the implant (length, 10 mm) was subdivided into three zones of equal width. The gross area of newly formed bone matrix in the central third of the cross-section was measured with a computer-assisted image analyzer (WinRoof; Mitani, Fukui, Japan).

Statistical analysis

Statistical significance of differences was analyzed by unpaired t test, using the statistical program StatView (version 5.0; SAS, Cary, NC). A p value of <0.05 was considered to indicate statistical significance.

RESULTS

Development of vascular network in the pores of IP-CHA

In all rats in the vascularized IP-CHA group, the inserted vascular pedicles displayed firm pulsation at the entrance of the IP-CHA block (Fig. 1, arrowhead). India ink perfusion produced dark stains on all surfaces of IP-CHA blocks, suggesting abundant blood flow from the pedicle inside the block to its outer surface. In contrast, in all animals in the control IP-CHA group, the surface of the implanted block was not stained by India ink.

In histological examination of the longitudinal cross-sections of the IP-CHA blocks, in the vascularized IP-CHA group, we observed many large blood vessels, which appeared to originate from the inserted vascular bundle, in the pores throughout the IP-CHA block. In the India ink perfusion experiment, most of the vessels in the pores of the vascularized IP-CHA group contained black ink particles, indicating that those vessels were effectively connected to the host circulation via the inserted vascular pedicle, providing an abundant blood supply (Fig. 2A, C, and E).

In the control IP-CHA group, fibrous tissues with microvessels were observed in the pores close to the outer surface of the block, but not in the deep pores. Furthermore, compared with the vascularized IP-CHA group, the fibrous tissues seen in the control IP-CHA group were markedly looser and the vessels were more immature and smaller. In those small vessels, very little India ink was seen, suggesting poor blood supply (Fig. 2B, D, and F).

In the vascularized IP-CHA group, immunostaining for von Willebrand factor clearly visualized blood vessels in almost every pore, suggesting a well-developed vascular network in the IP-CHA pores, due in part to interpore connections (Fig. 2C).

Effect of vascular bundle insertion on BMP-induced bone formation in IP-CHA

Histological examination of the longitudinal cross-sections of IP-CHA blocks loaded with 10 μg of rhBMP-2 showed that, in the vascularized BMP/IP-CHA group, there was abundant newly formed bone tissue in the pores. New bone formation was especially abundant in the pores close to the inserted vascular bundle; that is, far from the surface of the block. That newly formed bone tissue was accompanied by many large blood vessels that appeared to derive from the inserted vascular bundle (Fig. 3A and B). In the control BMP/IP-CHA group, most of the pores were filled with loose fibrous tissue with microvessels; a small amount of newly formed bone was observed in the pores close to the surface of the block at both ends, but not in the deep portion (Fig. 3C).

The average values ($\pm$standard deviation) for gross area of newly formed bone matrix in the pores of the central third were 1.0 ± 0.64 mm^2 in the vascularized BMP/IP-CHA group and 0.046 ± 0.054 mm^2 in the control BMP/IP-CHA group. The difference between these two values was statistically significant (Fig. 3D, $p < 0.05$).

In the experiment using a lower dose of rhBMP-2 (2 μg/block), we found no bone formation in the pores of IP-CHA blocks, with or without vascular insertion.

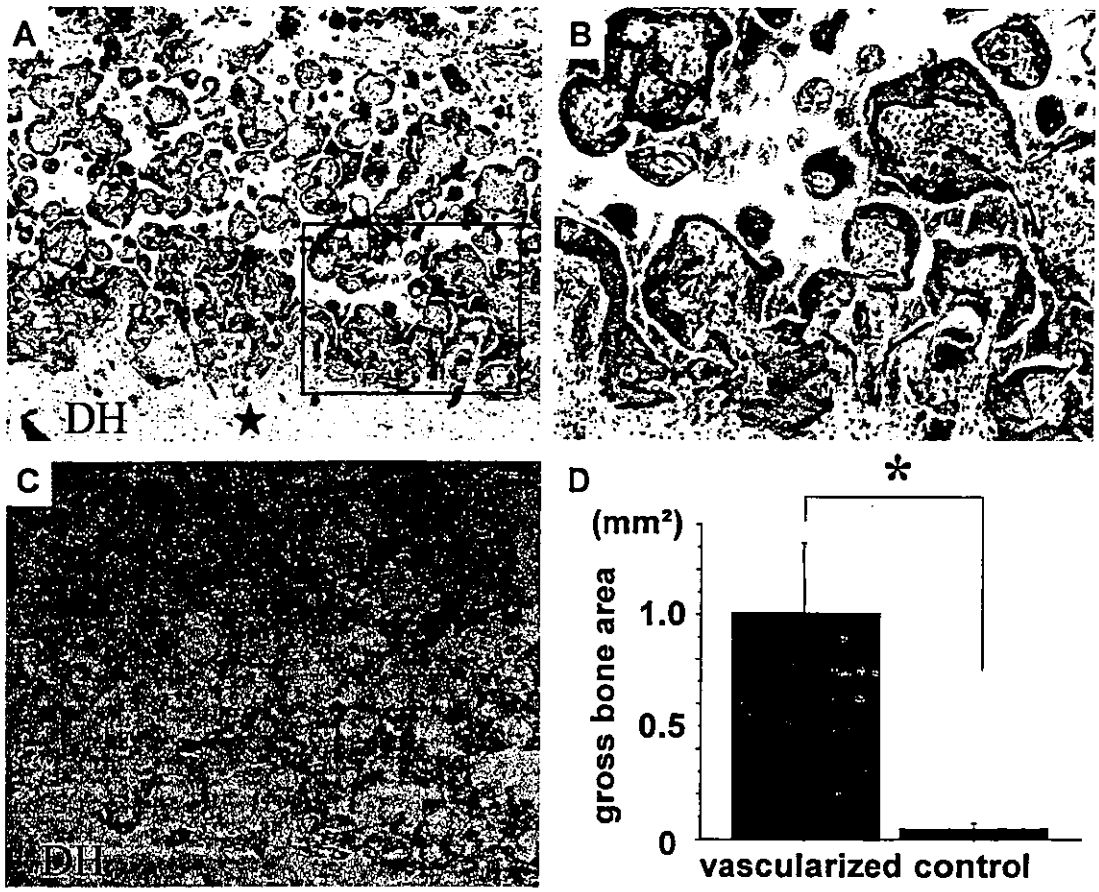

FIG. 3. Effect of vascular bundle insertion on bone formation in the deep portion of IP-CHA loaded with 10 μg of rhBMP-2. Representative microphotographs 3 weeks after subcutaneous implantation with (**A** and **B**) or without (**C**) vascular bundle insertion. (**A**) Abundant new bone formation with neovascularization was seen in the pores close to the longitudinal drill hole (**DH**), into which the superficial inferior epigastric vessels (star) were inserted (original magnification, ×40). (**B**) Higher magnification (×100) of the boxed area in (**A**). (**C**) Only minimal cellular invasion with microvessels was observed in the pores along the longitudinal drill hole (**DH**); no bone formation was observed (original magnification, ×40). (**D**) Histomorphometric results for the area of newly formed bone matrix in the central third of IP-CHA blocks. Vascularized, vascularized BMP/IP-CHA group (with vascular bundle insertion); control, control BMP/IP-CHA group (without vascular bundle insertion). Values represent the average area (mm^2) and standard deviations of four samples in each group. $*p < 0.05$.

DISCUSSION

Although porous ceramic bone substitutes made from calcium phosphate (e.g., HA) have been widely used in surgery to repair bone defects, their application is still limited because blood supply is essential for treatment of large bone defects and those with poor blood supply. In the present study, we found that insertion of a vascular bundle into IP-CHA produced a capillary vessel network in the pores. The present results indicate that, even when IP-CHA is implanted into a bone defect site with poor blood supply, insertion of a vascular bundle produces an abundant blood supply in most of the pores directly from the inserted vessels. The use of such implants appears to improve bone regeneration in bone defect sites.

In rigorous investigations of bone tissue-engineering techniques using bone matrix-producing cells or bone-inducible factors, porous HA was found to be a particularly suitable biomaterial for use as a scaffold.[11,15–19] It has been suggested that blood supply is an important element of bone tissue engineering, but no direct evidence of this has previously been reported. The present results, obtained using BMP-2 as the bone-inducible factor and IP-CHA as the scaffold, clearly demonstrate the essential role of blood supply in bone tissue engineering. The technique used in this study can also be used for cell-based bone tissue engineering; it is reasonable to assume that blood supply also plays an important role in cell-based bone tissue engineering.

There have been several studies in which a muscle flap was used as a source of blood supply for tissue engineering of bone.[20–24] However, this technique sacrifices

normal host muscle and, for recipient sites out of reach of a muscle flap, this technique is either not possible or requires vascular anastomoses. Because the present technique does not sacrifice any functional organ (including muscle), it could be used without affecting motor system function. Furthermore, this technique could be used to treat bone defects almost anywhere in the trunk and extremities, using local vessels. For example: for the femur, the deep femoral artery/vein bundle or inferior epigastric vessels could be used; for the humerus, deep brachial vessels; for the forearm, interosseous vessels.

In conclusion, the present results demonstrate that vascular bundle insertion into IP-CHA produces a vascular network in the porous structure, and that vascular bundle insertion enhances new bone formation in tissue-engineered bone, using rhBMP-2 and IP-CHA. Although further study is needed to clarify the clinical relevance of these findings, we believe that the present system of integrating a vascular network into IP-CHA is a useful technique for bone tissue engineering as a treatment for challenging orthopedic conditions.

ACKNOWLEDGMENTS

This work was supported in part by grants from the New Energy and Industrial Technology Development Organization (NEDO); the Ministry of Health, Labour, and Welfare, Japan; and the Ministry of Education, Culture, Sports, Science, and Technology, Japan. We thank Miss Kanae Asai for excellent technical assistance.

REFERENCES

1. Jarcho, M. Calcium phosphate ceramics as hard tissue prosthetics. Clin Orthop **157,** 259, 1981.
2. Bucholz, R., Carlton, A., and Holmes, R. Interporous hydroxyapatite as a bone graft substitute in tibial plateau fractures. Clin. Orthop. **240,** 53, 1988.
3. Uchida, A., Araki, N., Shinto, Y., Yoshikawa, H., Kurisaki, E., and Ono, K. The use of calcium hydroxyapatite ceramic in bone tumor surgery. J. Bone Joint Surg. Br. **72,** 298, 1990.
4. Nakano, K., Harata, S., Suetsuna. F., Araki, T., and Itoh, J. Spinous process-splitting laminoplasty using hydroxyapatite spinous process spacer. Spine **17,** 41, 1992.
5. Ayers, R.A., Simske. S.J., Nunes, C.R., and Wolford, L.M. Long-term bone ingrowth and residual microhardness of porous block hydroxyapatite implants in human. J Oral Maxillofac. Surg. **56,** 1297, 1998.
6. Mori, S., Yoshikawa, H., Hashimoto, J., Ueda, T., Funai, H., Kato, M., and Takaoka, K. Antiangiogenic agent (TNP-470) inhibition of ectopic bone formation induced by bone morphogenetic protein-2. Bone **22,** 99, 1998.
7. Kusumoto, K., Bessho, K., Fujimura, K., Akioka, J., Okubo, Y., Ogawa, Y., and Iizuka, T. The effect of blood supply in muscle and an elevated muscle flap on endogenous tissue-engineered bone by rhBMP-2 in the rat. Ann. Plast. Surg. **45,** 408, 2000.
8. Fujimura, K., Bessho, K., Kusumoto, K., Konishi, Y., Ogawa, Y., and Iizuka, T. Experimental osteoinduction by recombinant human bone morphogenetic protein 2 in tissue with low blood flow: A study in rats. Br. J. Oral Maxillofac. Surg. **39,** 294, 2001.
9. Taylor, G.I., Miller, G.D.H., and Ham, F.J. The free vascularised bone graft. A clinical extension of microsurgical technique. Plast. Reconstr. Surg. **55,** 533, 1975.
10. Weiland, A.J., Moore, J.R., and Daniel, R.K. Vascularised bone autografts. Clin Orthop. **174,** 87, 1983.
11. Quarto, R., Mastrogiacomo, M., Cancedda, R., Kutepov, S.M., Mukhachev, V., Lavroukov, A., Kon, E., and Marcacci, M. Repair of large bone defects with the use of autologous bone marrow stromal cells. N. Engl. J. Med. **344,** 385, 2001.
12. Tamai, N., Myoui, A., Tomita T, Nakase, T., Tanaka, J., Ochi, T., and Yoshikawa, H. Novel hydroxyapatite ceramics with an interconnective porous structure exhibit superior osteoconductive in vivo. J. Biomed. Mater. Res. **59,** 110, 2002.
13. Saito, N., Okada, T., Horiuchi, H., Murakami, N., and Takaoka K. A biodegradable polymer as a cytokine delivery system for inducing bone formation. Nat. Biotechnol. **19,** 332, 2001.
14. Nakase, T., Kaneko, M., Tomita, T., Myoui, A., Ariga, K., Sugamoto, K., Uchiyama, Y., Ochi, T., and Yoshikawa, H. Immunohistochemical detection of cathepsin D, K, and L in the process of endochondral ossification in the human. Histochem. Cell Biol. **114,** 21, 2000.
15. Norman, M.E., Elgendy, H.M., Shors, E.C., el-Amin, S.F., and Laurencin. C.T. An *in-vitro* evaluation of coralline porous hydroxyapatite as a scaffold for osteoblast growth. Clin. Mater. **17,** 85, 1994.
16. Kon, E., Muraglia, A., Corsi, A., Bianco, P., Marcacci, M., Martin, I., Boyde, A., Ruspantini, I., Chistolini, P., Rocca, M., Giardino, R., Cancedda, R., and Quarto, R. Autologous bone marrow stromal cells loaded onto porous hydroxyapatite ceramic accelerate bone repair in critical-size defects of sheep long bones. J. Biomed. Mater. Res. **49,** 328, 2000.
17. Petite, H., Viateau, V., Bensaid, W., Meunier, A., de Pollak, C., Bourguignon, M., Oudina, K., Sedel, L., and Guillemin, G. Tissue-engineered bone regeneration. Nat Biotechnol. **18,** 959, 2000.
18. Noshi, T., Yoshikawa, T., Ikeuchi, M., Dohi, Y., Ohgushi, H., Horiuchi, K., Sugimura, M., Ichijima, K., and Yonemasu, K. Enhancement of the in vivo osteogenic potential of marrow/hydroxyapatite composites by bovine bone morphogenetic protein. J. Biomed. Mater. Res. **52,** 621, 2000.
19. Boo, J.S., Yamada, Y., Okazaki, Y., Hibino, Y., Okada, K., Hata, K., Yoshikawa, T., Sugiura, Y., and Ueda, M. Tissue-engineered bone using mesenchymal stem cells and a biodegradable scaffold. J. Craniofac. Surg. **13,** 231, 2002.
20. Bernard, S.L., and Picha, G.J. The use of coralline hydroxyapatite in a "biocomposite" free flap. Plast. Reconstr. Surg. **87,** 96, 1991.
21. Kusumoto, K., Bessho, K., Fujimura, K., Akioka, J.,

Ogawa, Y., and Iizuka, T. Prefabricated muscle flap including bone induced by recombinant bone morphogenetic protein-2: An experimental study of ectopic osteoinduction in a rat latissimus dorsi muscle flap. Br. J. Plast. Surg. **51,** 275, 1998.

22. Casabona, F., Martin, I., Muraglia, A., Berrino, P., Santi, P., Cancedda, R., and Quarto, R. Prefabricated engineered bone flaps: An experimental model of tissue reconstruction in plastic surgery. Plast. Reconstr. Surg. **101,** 577, 1998.
23. Terheyden, H., Jepsen, S., and Rueger, D.R. Mandibular reconstruction in miniature pigs with prefabricated vascularized bone grafts using recombinant human osteogenic protein-1: A preliminary study. Int. J. Oral Maxillofac. Surg. **28,** 461, 1999.
24. Alam, M.I., Asahina, I., Seto, I., Oda, M., and Enomoto, S. Prefabricated vascularized bone flap: A tissue transformation technique for bone reconstruction. Plast. Reconstr. Surg. **15,** 952, 2001.

Address reprint requests to:
Akira Myoui, M.D.
Osaka University Graduate School of Medicine
Department of Orthopedics
2-2 Yamadaoka, Suita 565-0871, Japan

E-mail: myoi@ort.med.osaka-u.ac.jp

Cell Transplantation, Vol. 13, pp. 367–376, 2004
Printed in the USA.

0963-6897/04 $20.00 + .00

Bone Tissue Engineering Using Novel Interconnected Porous Hydroxyapatite Ceramics Combined With Marrow Mesenchymal Cells: Quantitative and Three-Dimensional Image Analysis

Masataka Nishikawa,* Akira Myoui,* Hajime Ohgushi,† Masako Ikeuchi,†
Noriyuki Tamai,* and Hideki Yoshikawa*

*Department of Orthopaedics, Osaka University Graduate School of Medicine,
2-2 Yamadaoka, Suita City, Osaka 565-0871, Japan
†Tissue Engineering Research Center, National Institute of Advanced Industrial Science and Technology,
3-11-46 Nakouji, Amagasaki City, Hyogo 661-0974, Japan

We developed fully opened interconnected porous calcium hydroxyapatite ceramics having two different pore sizes. One has pores with an average size of 150 μm in diameter, an average 40-μm interconnecting pore diameter, and 75% porosity (HA150). The other has pores with an average size of 300 μm in diameter, an average 60–100-μm interconnecting pore diameter, and 75% porosity (HA300). Because of its smaller pore diameter, HA150 has greater mechanical strength than that of HA300. These ceramics were combined with rat marrow mesenchymal cells and cultured for 2 weeks in the presence of dexamethasone. The cultured ceramics were then implanted into subcutaneous sites in syngeneic rats and harvested 2–8 weeks after implantation. All the implants showed bone formation inside the pore areas as evidenced by decalcified histological sections and microcomputed tomography images, which enabled three-dimensional analysis of the newly formed bone and calculation of the bone volume in the implants. The bone volume increased over time. At 8 weeks after implantation, extensive bone volume was detected not only in the surface pore areas but also in the center pore areas of the implants. A high degree of alkaline phosphatase activity with a peak at 2 weeks and a high level of osteocalcin with a gradual increase over time were detected in the implants. The levels of these biochemical parameters were higher in HA150 than in HA300. The results indicate that a combination of HA150 and mesenchymal cells could be used as an excellent bone graft substitute because of its mechanical properties and capability of inducing bone formation.

Key words: Bone tissue engineering; Hydroxyapatite; Image analysis; Marrow mesenchymal cell; Osteoblast; Osteoconduction

INTRODUCTION

The ideal bone graft is autogenous bone but there are many problems, such as quantitative limitations of the graft and the inevitable invasion of normal tissues to harvest the graft bone. To avoid these problems, synthetic hydroxyapatite (HA) ceramics have been used as bone graft substitutes in orthopedic, craniofacial, and dental applications (1,3,7,10,21). HA ceramics are known to be biocompatible, osteoconductive, and bioactive, with bone bonding directly to the surface of the ceramics (4,8,22). However, only a few researchers have reported that the pores of implanted ceramics were completely filled with the newly formed host bone (22). It would be reasonable to assume that the reason for this is the nonuniform pore geometry and few interpore connections of conventional synthetic HA ceramics. The size of the interpore connections rather than the size of the pores themselves might be the primary limiting factor of osteoconduction into the central area of HA ceramic blocks. This is because interpore connections under 3 μm in diameter do not permit cell migration and vascularization into the pores, events essential for new bone formation (20).

We recently developed fully open interconnected porous calcium hydroxyapatite ceramics (IP-CHA) and reported the resulting superior osteoconduction by permitting cells and tissues to invade deep into the pores (20). However, not all of these ceramics are osteoinductive and, therefore, the applications are limited. In this re-

Address correspondence to Hajime Ohgushi, M.D., Ph.D., Tissue Engineering Research Center, National Institute of Advanced Industrial Science and Technology, 3-11-46 Nakouji, Amagasaki City, Hyogo 661-0974, Japan. Tel: (+81) 6-6494-7806; Fax: (+81) 6-6494-7861; E-mail: hajime-ohgushi@aist.go.jp

gard, we have reported on the osteogenic capability of fresh marrow cells or culture-expanded marrow mesenchymal cells, which combined with porous HA ceramics. Such composites showed ectopic bone formation in the pore areas of the HA ceramics (11,13,14,18,24,25). Importantly, the composites also demonstrated their healing potential when implanted into a site in which there is a bony defect (12). Due to the interconnected porous structure of IP-CHA, osteogenic cells can be appropriately introduced within the pores and are thus useful as a scaffold in bone tissue engineering. In this study, IP-CHA, having two different pore sizes, were combined with marrow mesenchymal cells and evaluated for their osteogenic capability.

MATERIALS AND METHODS

Materials

Fully open IP-CHA were synthesized by adopting a "foam-gel" technique from a slurry of hydroxyapatite (60 wt%) with a cross-linking substrate (polyethyleneimine, 40 wt%), as previously reported (20). The solid and porous components of the microstructure were completely interconnected. We prepared two types of IP-CHA. One had pores averaging 150 μm in diameter, an average 40-μm interconnecting pore diameter, and 75% porosity (HA150). The other had pores averaging 300 μm in diameter, 60–100-μm interconnecting pore diameter, and 75% porosity (HA300).

For comparison, we purchased three different commercially available synthetic porous hydroxyapatite ceramics (HA-A, HA-B, and HA-C), which have been used in orthopedic or dental surgery in Japan. HA-A has an average pore diameter of 300 μm and 50% porosity. HA-B has an average pore diameter of 200 μm and 70% porosity. HA-C has pore with diameters of 50–300 μm and 35–48% porosity.

Blocks of these ceramics (HA150, HA300, HA-A, HA-B, and HA-C) were cut and shaped into 5-mm-diameter disks that were 2 mm thick.

Mercury Porosimetry

The distribution of the interpore connections in hydroxyapatite ceramics was measured from the penetration of Hg liquid in an evacuated porosimeter (pore sizer, 9310, Shimadzu Co., Kyoto, Japan) as previously described by Tamai et al. (20). The available pores that were connected by interpore connection >10 μm in diameter were calculated by the following equation: available porosity (%) = total porosity (%) − unavailable porosity (%) (the inaccessible pore space calculated by integrating the cumulative volume of pores that were connected with interpore connections <10 μm in a diameter, according to the result of mercury porosimeter).

Marrow Cell Preparation and Culture

Marrow cells were obtained from the bone shaft of the femora of 7-week-old Fischer 344 male rats. Both ends of the femur were cut away from the epiphysis, and the marrow was flushed out using 10 ml of culture medium expelled from a syringe through a 21-gauge needle, according to the method developed by Maniatopoulos et al. (9). The released cells were collected in two T-75 flasks (Costar, Cambridge, MA) containing 15 ml of the standard medium described below. The medium was changed after 24 h to remove hematopoietic cells. Subsequently, the medium was renewed three times a week. Cultures were maintained in a humidified atmosphere of 95% air with 5% CO_2 at 37°C.

The standard medium consisted of Eagle's minimal essential medium (MEM) containing 15% fetal bovine serum (JRH Bioscience, Lenexa, KS, Lot No.002095) and antibiotics (100 U/ml of penicillin, 100 μg/ml of streptomycin, and 0.25 μg/ml of amphotericin B; Sigma Chemical Co., St. Louis, MO).

After 7 days in primary culture, adherent marrow mesenchymal cells (MMCs) were released from the culture substratum using 0.1% trypsin. The cells were concentrated by centrifugation at 900 rpm for 5 min at 4°C and resuspended at 10^6 cells/ml. The 24 ceramic disks were soaked in 4 ml of cell suspension (10^6 cells/ml) overnight in a CO_2 incubator.

After the overnight incubation, the disks were transferred into a 24-well plate (Falcon, Franklin Lakes, NJ) for subcultures. Each ceramic was subcultured in one well with 1 ml of the standard medium supplemented with 10 mM of β-glycerophosphate, disodium salt, pentahydrate (Calbiochem, Darmstadt, Germany), 82 μg/ml of L-ascorbic acid phosphate magnesium salt *n*-hydrate (Wako Pure Chemical Industrials, Osaka, Japan), and 10^{-8} M of dexamethasone (Dex, Sigma Chemical Co.). To evaluate the efficiency of the dexamethasone, the subcultures without Dex were used as in vitro controls. The medium was renewed three times a week, and the subcultures were maintained for 2 weeks. These subcultured MMCs in the ceramic disks were washed twice with phosphate-buffered saline (Gibco, Invitrogen Corporation, Grand Island, NY) and prepared for measurement of alkaline phosphatase (ALP) activity to evaluate if the HA ceramics support in vitro osteoblastic differentiation of marrow mesenchymal cells.

Implantation

Syngeneic 7-week-old male Fischer 344 rats were anesthetized by intramuscular injection of ketamine (45 mg/kg) and xylazine (9 mg/kg). Five ceramic disks cultured with MMCs in the presence of Dex for 2 weeks were implanted subcutaneously at five sites into the back of each syngeneic rat and five ceramic disks with-